The Thesis Committee for Bishwas Ghimire
Certifies that this is the approved version of the following thesis:

Modeling Formation Resistivity Changes During Leak-Off Tests (LOT's)

APPROVED BY
SUPERVISING COMMITTEE:

Supervisor: _____
Hugh Daigle

Co-Supervisor: _____
Kenneth Gray

Modeling Formation Resistivity Changes During Leak-Off Tests (LOT's)

by

Bishwas Ghimire, B.S.

Thesis

Presented to the Faculty of the Graduate School of

The University of Texas at Austin

in Partial Fulfillment

of the Requirements

for the Degree of

Master of Science in Engineering

The University of Texas at Austin

December 2015

Dedication

This work is dedicated to my parents, Chunnu Ghimire and Bijaya Raj Ghimire, and my elder brother, Gaurav Ghimire for their love, support, and guidance that have made it possible for me to come this far in life.

Acknowledgements

I would like to extend my deepest and sincerest gratitude towards my supervisors, Dr. Daigle and Dr. Gray, for guiding and supporting me from the very beginning to make my graduate school experience an awesome learning experience. Their valuable advice and insightful comments along the way have made my journey as a graduate student a lot easier and more productive than it would have been without them.

I would also like to thank my colleagues in the Wider Windows group, who have evaluated my work multiple times during its progress and contributed with their useful discussions and suggestions for improvement.

Finally, I would like to thank all the sponsors of the Wider Windows Industry Affiliate Program - BHP Billiton; British Petroleum; Chevron; ConocoPhillips; Marathon Oil Company; National Oilwell Varco; Occidental Oil and Gas; and Shell. Their funding has made this work possible. In addition to that, the insightful feedbacks and guidance provided by their representatives during our review meetings have been tremendously helpful for my project.

Abstract

Modeling Formation Resistivity Changes during Leak-Off-Tests (LOT's)

Bishwas Ghimire, M.S.E

The University of Texas at Austin, 2015

Supervisors: Hugh Daigle, Kenneth Gray

Leak-Off-Tests (LOT's) are performed shortly after drilling into the new formation below a cased interval in order to determine the strength of the formation below the cased interval. This helps determine the upper limit of mud weight that can be used safely while drilling the next section, without risking formation breakdown and lost circulation. During LOT, well is shut in, and drilling fluid is pumped into the wellbore by a surface pump. As wellbore pressure increases due to pumping, the entire wellbore system including the formation first responds by expanding. When the wellbore pressure goes beyond a critical value called Leak-Off Pressure (LOP), drilling fluid starts to leak into the formation in the open hole section, first through porous flow and then, through fractures that are induced at the wellbore due to high pressure. This leakage of drilling fluid from the wellbore into the formation along with formation deformation can cause many changes in formation resistivity.

Typically, formation resistivity depends on formation water saturation and salinity, and porosity through Archie's equation. Hence, any change in resistivity can be modeled by modeling deformation and invasion during LOT. In this study, a poro-elastic model has been developed to investigate the resistivity change around wellbore during LOT by coupling the effects of deformation and invasion that occur as pressure builds up in the wellbore. Having a model to obtain resistivity around the wellbore during LOT is a prerequisite to predicting the resistivity tool response of a given tool during LOT. By predicting resistivity response during LOT and matching with measured field data, important properties of the formation like permeability and compressibility can be determined. The model developed assumes porous flow around the wellbore to determine the true formation resistivity during initial LOT pressure buildup by coupling the effects of deformation and invasion manifested in the formation in terms of change in formation porosity, water salinity, and water saturation. The results show that the effects of deformation on formation resistivity are relatively small, and while salinity mostly controls formation resistivity in a completely water-saturated zone, water saturation becomes a more important variable in an arbitrarily saturated zone with changing water saturation.

Table of Contents

List of Tables

List of Figures

List of Illustrations

Chapter 1: Introduction

1.1 Motivation

Leak-Off Tests (LOT's) are performed shortly after commencing drilling on a new section of open hole below a cased interval with a purpose to determine the upper window of the mud weight that may be safely used without risking lost circulation and related formation damage. Usually, LOT's are performed by shutting in the well and pumping in drilling fluid to increase pressure in the wellbore. As pressure in the wellbore increases, some of the drilling fluid will bleed into the formation by porous flow, but since the wellbore pressure increases much faster than it can be equalized by porous flow, eventually the rock around the wellbore fails, opening fractures and allowing the drilling fluid to leak off into the formation. Thus, LOT provides information about formation strength and integrity, which is vital to drilling the next section safely.

During the initial pressure buildup of LOT, increase in wellbore pressure causes deformation of the formation as well as some porous flow of drilling fluid into the formation due to the pressure gradient. When the borehole pressure reaches the fracture initiation pressure, the formation yields and fractures initiate and propagate, allowing drilling fluid to leak off more rapidly into the formation. Even though fractures primarily are responsible for fluid leak-off after fracture initiation, since fractures are significantly more complex to model, we are modeling the initial pressure build-up phase prior to fracture initiation when only porous flow occurs around the wellbore. This is also done for the sake of simplicity of the model. Thus, in this study, uniform porous flow of

drilling mud into the formation during LOT is used as an effective phenomenon that, on average, sums up the leakage behavior during the pressure build up phase of the LOT.

Logging-While-Drilling (LWD) Resistivity-at-the-bit (RAB) tools may be inserted in the drilling string during LOT to gather resistivity measurements at multiple depths of investigation (DOI). These tools are designed to operate under high pressure and can provide valuable information on formation properties and deformation during LOT's. Since resistivity of a formation is a function of the volume of conductive fluids present in the formation, effects of deformation and invasion during LOT are manifested as changes in resistivity of the formation around wellbore. Hence, evolution of resistivity around wellbore can be used to study how drilling fluid is invading the formation and how the formation is deforming due to pressure gradient. This, in turn, may be used to determine valuable information on permeability and compressibility of the formation, which are important parameters for any drilling program and completion design.

The objective of this thesis is to investigate how resistivity changes around wellbore due to invasion and deformation that occur during LOT. Effect of deformation is investigated using a finite element model in ABAQUS, and effect of invasion is incorporated using radial flow around wellbore. The two effects are then coupled to allow for the investigation of resistivity at any point radially outward in the formation during LOT. For specified drilling fluid and formation water resistivities, the true resistivity value at each point in the formation is determined. This, in future, will allow for the determination of expected RAB tool response of a laterolog resistivity measurement of the formation by solving response functions for particular electrodes'

setting in the tool (Cozzolino & da Silva, 2007; Pardo, Calo, Torres-Verdin, & Nam, 2008; Nam, Pardo, & Torres-Verdín, 2008). Predicted response can then be compared with measured field data to determine important properties of the formation like compressibility and true resistivity through an inversion method. Although RAB measurements are not routinely run during LOT, it is anticipated that this proof of concept will encourage the industry to run field trails with LWD RAB tools during LOT.

1.2 Thesis Organization

This thesis has 6 chapters. Chapter 1 mainly discusses the motivation behind this work. Chapter 2 touches on the relevant concepts that are important in understanding LOT and resistivity change during LOT and previous work done in this area from the literature. Chapter 3 thoroughly describes the approach that is used to model resistivity change around wellbore during LOT. It takes different scenarios into account: water-saturated formations, oil-saturated formations, and arbitrarily saturated formations; and describes how each can be handled with our approach. Chapter 4 is solely dedicated to work done using Finite Element Method (FEM) in ABAQUS to model the effects of deformation during LOT. Chapter 5 discusses the results, and Chapter 6 concludes the thesis along with some directions for future work.

Chapter 2: Relevant Concepts and Literature Overview

2.1 Leak-Off Tests (LOT's)

Before commencing drilling in a new open-hole section below a cased interval, it is crucial to determine the strength of the exposed formation to ensure that the next section can be drilled safely without any risk of formation breakdown. That's why LOT is run as a common procedure during drilling as it tells us the maximum pressure that a formation can withstand without fracturing. This maximum pressure corresponds to an equivalent mud weight that cannot be exceeded in order to prevent fractures and more importantly, lost circulation, which has presented itself, for the past century, as one of the most expensive drilling-related challenges in the petroleum industry, both in terms of cash and rig time (Wang, et al., 2008). Hence, LOT estimates the upper window of mud weight that can be used safely while drilling. Putting this in other words, LOT determines the formation fracture gradient that is critical to ensure safe drilling practice.

During LOT, the well is shut in, and drilling mud is pumped into the formation using a pump at the surface. Usually, the mud is pumped at a constant rate, and pressure is allowed to increase in the wellbore. This increase in pressure causes the formation to deform and mud to leak into the formation first via porous flow and then through fractures once the wellbore pressure reaches fracture initiation pressure. The amount of fluid that actually leaks into the formation is significantly less than the total fluid that is pumped from the surface, because a considerable amount of mud volume is taken up by mud compression, casing expansion, borehole expansion, and cement and formation expansion (Fu, 2014). There are several models that take these subsystems into account to come up with the fluid volume that is actually leaking into the formation as LOT progresses. One of these models shall be used in this work to model leakage volume,

which is a crucial parameter in this study. But first, a typical LOT plot has to be studied in order to understand the basic concepts that are relevant during LOT.

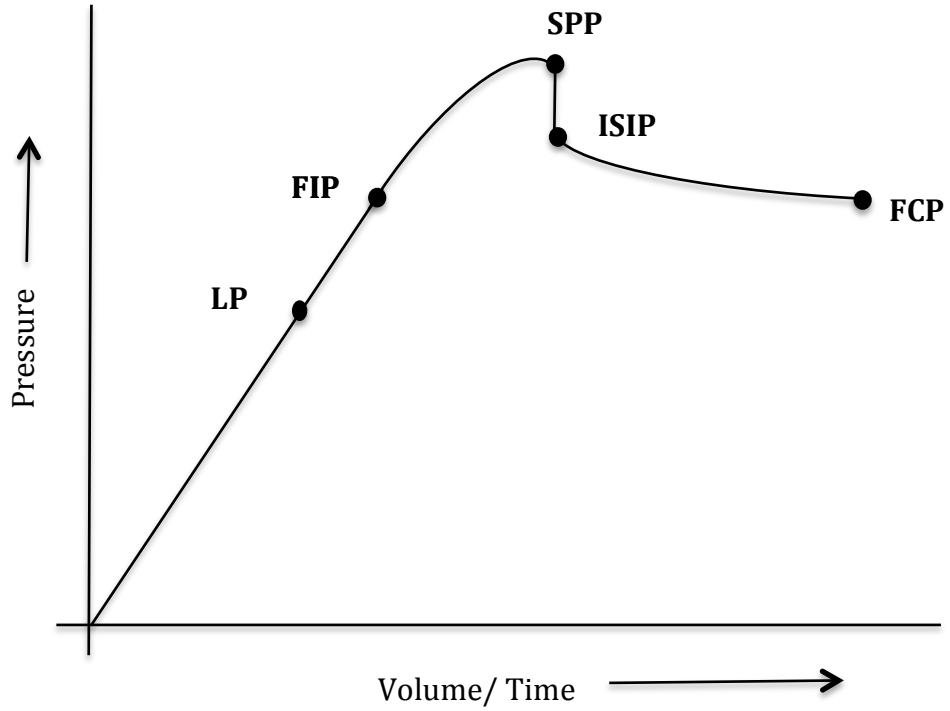

Fig 2.1 Schematic of a typical LOT plot (Modified after Postler (1997))

Above is a schematic of a typical LOT plot, very similar to the one illustrated by Postter (1997). As seen in the plot, initial pressure build-up during LOT is linear. After the pressure in the wellbore builds up to a certain value called Fracture Initiation Pressure (FIP), fractures initiate, and fluid starts leaking off more rapidly into the formation causing the pressure curve to bend down slightly (Postler, 1997). This change of slope can also be interpreted as a sudden increase in the compressibility of the system due to leaking fluid that causes the rate of pressure buildup to decline rapidly (Addis, Hanssen, Yassir, Willoughby, & Enever, 1998).

As mud is lost into the formation through open fractures, pressure is released at the wellbore. As mentioned above, this response is felt at the surface as shown by the changing slope of the pressure curve. Many of the recent studies agree with Postler's hypothesis that deviation of the pressure build up curve from linearity marks the opening of the first small stable fracture at the wellbore wall in the open hole (Okland, Gabrielsen, Gjerde, Koen, & Williams, 2002; Lee, Bratton, & Birchwood, 2004; van Oort & Vargo, 2007; Li, Lorwongngam, & Roegiers, 2009; Aadnoy, Mostafavi, & Hareland, 2009; Heger & Spoerker, 2011).

FIP is commonly also referred to as leak-off pressure (LOP), since fluid leak-off is commonly believed to start after fracture initiation. However, it is sometimes suggested that LOP represents formation intake pressure, not FIP, and only pumping beyond LOP will cause fractures at the wellbore (Aadnoy, Mostafavi, & Hareland, 2009).

While the drilling fluid bleeds into the formation beyond FIP, pumping is continued further until pressure reaches Stop-Pump Pressure (SPP) at which point pump is stopped. The equivalent mud weight (EMW) at SPP is reported as the strength of the casing shoe (van Oort & Vargo, 2007). In case if pumping is not stopped in time, pressure in the wellbore can reach formation breakdown pressure (FBP) at which point formation breaks down, and lost circulation occurs. If this happens, pumping is stopped promptly right after at SPP. SPP is the highest pressure that is achieved during LOT. As soon as the pump stops, pressure falls down instantaneously to a lower value called instantaneous shut-in pressure (ISIP). Postler considered ISIP to be a good estimation of the minimum formation stress, as it represents the stresses at the tip of LOT-induced fractures that supposedly extend to far-field region (Postler, 1997). After stopping the pump, well is shut in, and pressure is allowed to stabilize. In this shut-in period, fractures start to close, and wellbore pressure starts to stabilize at Fracture Closure Pressure (FCP).

There is still a slight reduction in pressure during the shut-in period due to the loss of drilling fluid into the permeable formation (Postler, 1997).

Limit Pressure (LP) is the pressure limit set for Formation Integrity Test (FIT). If the formation fracture gradient has already been well characterized like they are in mature fields, FIT is performed just to verify formation integrity. The limit is usually set below the previously characterized FIP to avoid fracture formation and to prevent risks of lost circulation.

Sometimes, extended LOT's, popularly called XLOT's, are performed in which drilling mud is pumped into the formation in multiple LOT cycles. These tests are usually done to better characterize fracture gradient by investigating fracture growth, propagation, closure, and reopening.

2.2 LOT models

One of the key parameters that go into determining how drilling fluid is invading the formation during LOT is the amount of drilling fluid that is actually leaking into the formation. When the well is shut in and drilling fluid is pumped into the wellbore from the surface, pressure starts to increase in the wellbore. This increase in pressure results in fluid leaking into the formation first via porous flow and then through fractures. In addition to the mud leaking into the formation, a significant amount of pumped mud goes into subsystems like mud compression, casing and borehole expansion, cement and formation expansion, etc. These should be taken into account while determining the volume of mud that is actually leaking into the formation. Several models have been proposed in the literature to address this issue, out of which some will be discussed below

including the one that will be used in this study. A more thorough study of these models can be found in Fu's thesis on LOT models (Fu, 2014).

2.2.1 Altun LOT model (1999)

Altun model was first proposed by Altun in his PhD dissertation to better analyze LOT data taking into account the non-linear relationship between observed pump pressure and volume of mud pumped (Altun, 1999). A comprehensive and mathematical LOT model was developed subsequently, and the model was applied to predict the observed non-linear behavior of field some examples (Altun, Langlinais, & Bourgoyne Jr., 2001). Altun LOT model consists of 4 subsystems that are accountable for the total mud pumped into the formation during LOT: mud compression, casing expansion, borehole expansion, and fluid leakage (Altun, Langlinais, & Bourgoyne Jr., 2001). Each subsystem is investigated separately to determine the mud volume contribution of that subsystem. In the end, contributions from each of the four subsystems are summed up to model the total pumped volume.

Mud compression volume is simply obtained as the product of compressibility of mud, total pumped volume, and pump pressure. Casing expansion is modeled using a concentric cylinder approach where the pressure condition at the inner and outer casing radii is used to determine the expansion volume of the casing string. In order to account for the compression of mud that occupies the expansion volume of the casing string, mud compression expression is invoked once again to calculate the volume pumped to compress the casing expansion volume.

Borehole expansion volume is determined in a similar manner using pressure conditions in the open hole. Mud pumped to compress the borehole expansion volume is determined as well.

Leakage volume in Altun model is estimated using Poiseuille's flow in channels. In this model, volume leaking into the formation depends on the pressure differential across the flow channel formed during LOT. A leak constant is used which is a function of the geometry of flow channels and properties of leaking mud.

$$V_f = D\Delta Pt \tag{2.1}$$

where,

$V_f = Leak\ volume$

$\Delta P = Pressure\ drop$

$t = Time$

$D = Leak\ constant$

Leak constant has various forms depending upon the flow model and channel geometry. For rectangular flow channels modeled under Poiseuille's law, which Altun model uses, leak constant takes the following form in field units.

$$D = 8.7(10^9)\frac{W^2 A_{xz}}{\mu L} \tag{2.2}$$

where,

$W = Width\ of\ the\ fracture$

$A_{xz} = Cross - sectional\ area\ of\ the\ fracture$

$\mu = Leak\ fluid\ viscosity$

$L = Channel\ length$

In summary, the total pumped volume during LOT is the sum of contributions from different subsystems that can be summarized as shown below (Altun, Langlinais, & Bourgoyne Jr., 2001):

$$\begin{aligned} \text{Volume pumped} = {} & \text{Mud compression volume} \\ & + \\ & \text{Casing expansion volume} \\ & + \\ & \text{Volume to compress casing expansion volume} \\ & + \\ & \text{Borehole expansion volume} \\ & + \\ & \text{Volume to compress borehole expansion volume} \\ & + \\ & \text{Leakage volume} \\ & + \\ & \text{Volume to compress leakage volume} \end{aligned}$$

Of these contributions, it was calculated and concluded that only casing expansion volume and leakage volume are the most important ones as they contribute most of the pumped volume during LOT. Other contributions from terms of the volume to compress

casing- expansion-volume, the volume to expand the borehole, the volume to compress borehole-expansion-volume, and the volume to compress the leakage volume altogether account for less than 1% of the volume pumped into the system, even in extreme cases; so, these contributions are negligible and can be safely ignored (Altun, Langlinais, & Bourgoyne Jr., 2001). With this assumption, Altun et al. came up with an exact expression to model the total system behavior during LOT, which can be summarized by Eq. 2.3. The first term in Eq. 2.3 accounts for the compression of drilling fluid and any fluid leakage, and the second term accounts for casing expansion.

$$V = \frac{V_o(e^{c_m P}-1)}{1-\frac{D}{q}P} + 2\pi h_{csg} R_i^2 \frac{P}{E_{csg}} \left[\frac{R_o^2+R_i^2}{R_o^2-R_i^2}(1-\nu^2) - (\nu+\nu^2)\right] \quad (2.3)$$

where,

$V = Total\ volume\ pumped$

$V_o = System\ volume$

$c_m = Compressibility\ of\ mud$

$P = Pump\ pressure$

$D = Leak\ constant$

$q = Leak\ rate$

$h_{csg} = Casing\ height$

$E_{csg} = Casing\ Young's\ modulus$

$\nu = Casing\ Poisson's\ ratio$

$R_i, R_o = Inner\ and\ outer\ radii\ of\ casing\ string$

Altun LOT model does have its own pros and cons. The biggest advantage of Altun LOT model is that it is the first model that attempts to characterize the non-linear

behavior during LOT using a complete mathematical approach. A downside is that even though casing expansion is included, the fact that casing string comes in layers is ignored. Also, expansion volumes of cement and formation rock outside the casing string, which cannot be trivially neglected, are not considered by Altun LOT model while calculating expansion volumes.

2.2.2 Paknejad LOT model (2007)

Paknejad et al introduced another LOT model in 2007 to evaluate LOT's in shallow marine sediments (Paknejad, Schubert, & Amani, 2007). This is commonly referred to as Paknejad LOT model here. Paknejad LOT model is very similar to Altun LOT model in terms of how mud compression and casing and borehole expansion are handled; however, Paknejad LOT model handles leakage volume very differently. Drilling mud is assumed to leak through vertical fractures initiated during LOT. The expression for pressure drop in the fluid leaking through these fractures is then obtained using hydraulic fracture theory.

$$\Delta P = \frac{4.064qB}{h_f x_f}\sqrt{\frac{\mu t}{k\phi c_t}} \tag{2.4}$$

where,

$\Delta P = Pressure\ drop\ in\ fractures$

$q = Injection\ rate$

$t = Injection\ time$

$B = Formation\ volume\ factor$

$h_f = Fracture\ height$

$x_f = Fracture\ half\ length$

$\mu = Fluid\ viscosity$

$k = Permeability$

$\phi = Porosity$

$c_t = Total\ compressibility$

The deficiencies of Altun model remain in Paknejad model.

2.2.3 Wider Windows LOT model

Wider Windows LOT model is the model that has been used in this work to obtain leakage volume during LOT. Both Altun and Paknejad LOT models neglect the expansion volumes of cement sheath and formation rock beyond the casing string. These volumes are not actually trivial and shouldn't be neglected. To overcome this deficiency of previous models, Wider Windows LOT model was developed by Yao Fu in 2014 (Fu, 2014). Wider Windows LOT model is an enhanced Altun model, which, in addition to the four subsystems in Altun model, includes two more subsystems to incorporate the volume contribution due to cement sheath expansion and formation expansion outside the casing. This is summarized in the following expression.

Volume pumped = Mud compression volume

+

Casing expansion volume

+

Volume to compress casing expansion volume

+

Borehole expansion volume

+

Volume to compress borehole expansion volume

+

Leakage volume

+

Volume to compress leakage volume

+

Cement sheath expansion volume

+

Volume to compress cement sheath expansion volume

+

Formation rock expansion volume

+

Volume to compress formation rock expansion volume

Wider Windows LOT model uses Norris's approach to determine the expansion volumes of casing string, cement, and formation rock (Norris). 20" casing, cement, and formation rock are modeled as multiple concentric cylinders, and using Norris' method, which enforces kinematic compatibility constraint (radial deflection at the outer surface of one cylinder is equal to the radial deflection of the inner surface of adjacent cylinder) across the interface of any two cylinders, deflection of each cylinder is obtained. It should be noted that the outermost cylinder that models formation rock is assumed to be of thickness equal to six times the wellbore radius to ensure that stress on the outer surface is not affected by wellbore distortion (Fu, 2014).

Leak volume, borehole expansion volume, and mud compression volumes are determined using methods similar to Altun's method. This is why Wider Windows LOT model can be thought of as an extension of Altun LOT model. Wider Windows LOT model is also capable of including any conductor casing that might be present in the system to account for its volume contribution. In fact, in a few calculations done using Wider Windows LOT model, Fu assumes conductor casing up to several depths to compare the results (Fu, 2014).

Result from Wider Windows LOT model has been used as one of the variables in our resistivity model in the form of leakage volume during LOT.

Below are some figures of the results from Fu's thesis that can visually summarize how Wider Windows LOT model works. Fig 2.2 shows the contribution from each subsystem towards total mud volume that is pumped during LOT.

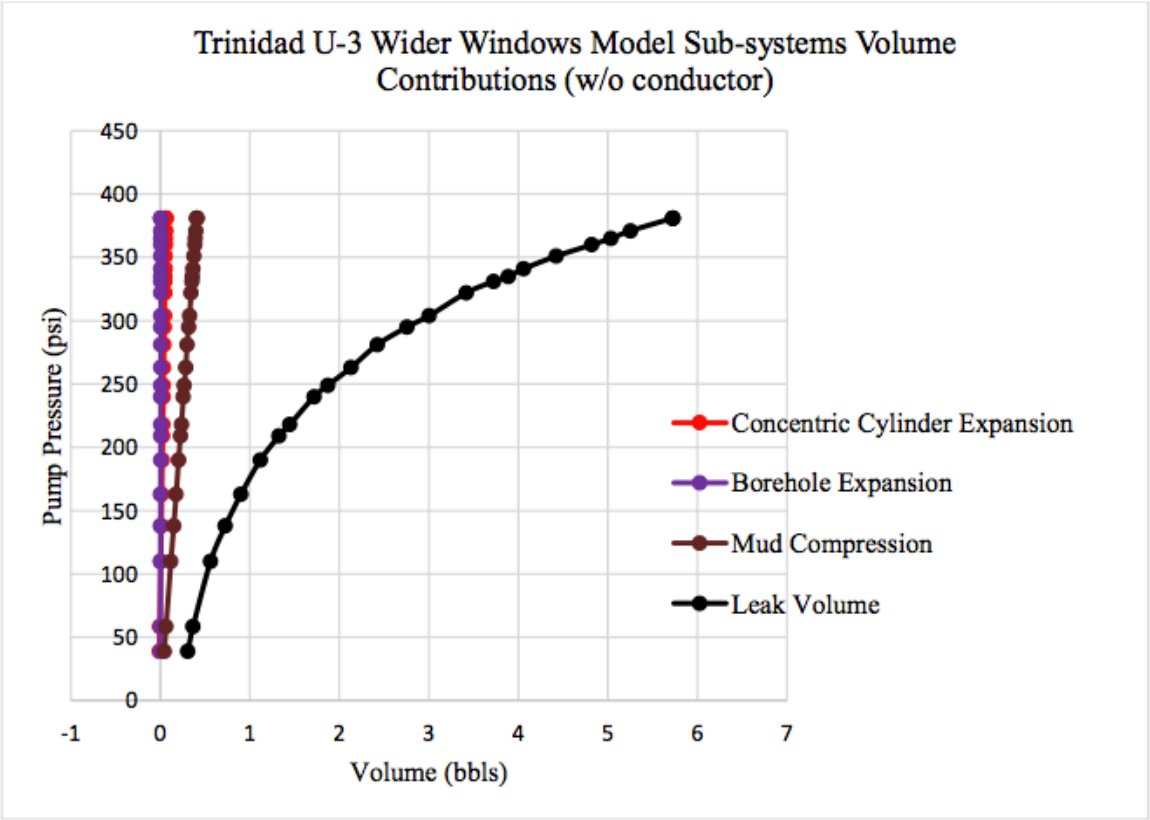

Fig 2.2 Trinidad U-3 Wider Windows model subsystem volume contribution (Fu, 2014)

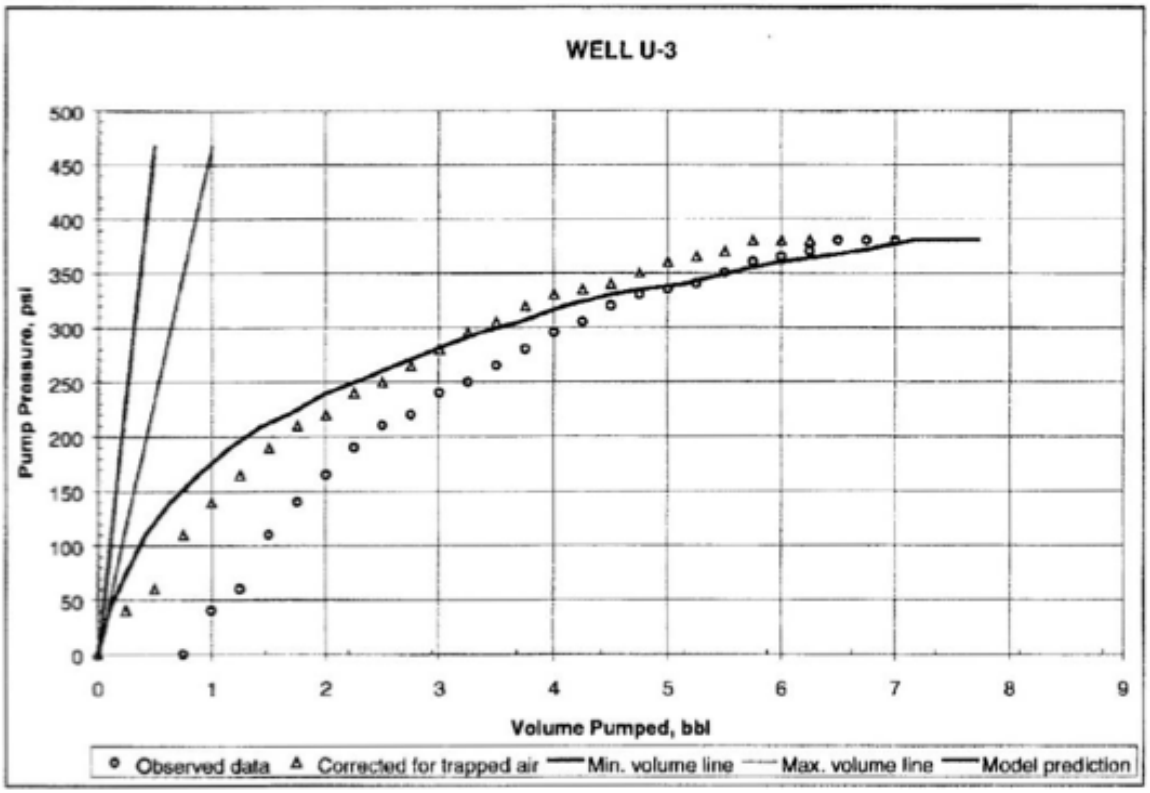

Fig 2.3 Altun model prediction for Trinidad U-3 (Altun, 2001)

Fig 2.3 shows the original LOT data for Trinidad U-3 and prediction by Altun model. Trinidad U-3 is one of the three offshore wells that Altun used in his study for his dissertation. The data has been digitized by Fu (2014) and used in his work to test Wider Windows LOT model. Some parameters that are not available, but are required to complete the model definition, have been assumed within practical limits. Resulting data from Wider Window LOT model's application to Trinidad U-3 has been used in our study while demonstrating the method to investigate resistivity change around wellbore

during LOT. Other available data Trinidad U-3 related to well, drilling mud, and formation are used, if needed, in our study of resistivity. Some parameters have been used assumed as per our necessity as well.

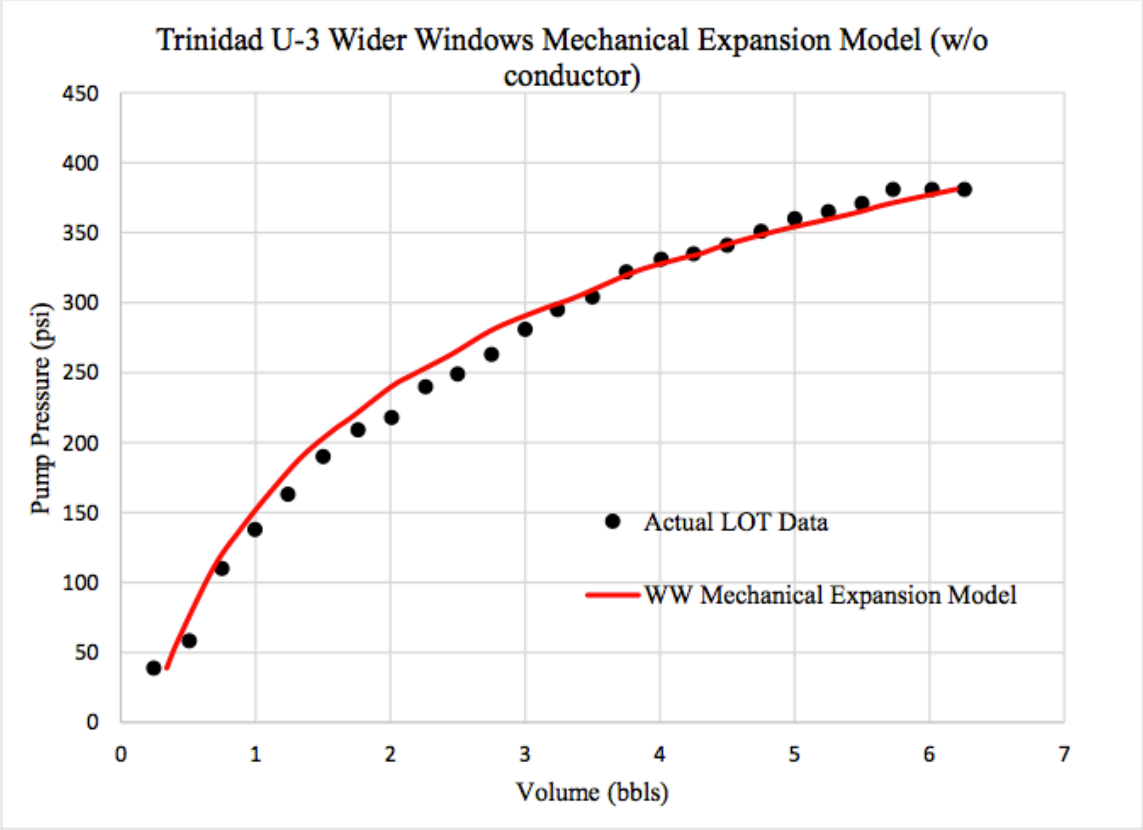

Fig 2.4 Wider Windows LOT model (w/o conductor casing) prediction for Trinidad U-3 (Fu, 2014)

Fig 2.4 shows the predicted LOT mud volume by Wider Windows LOT model without including conductor casing in the model. Wider Windows LOT model shows a good agreement with observed LOT data, hence it is used to obtain leakage volume during LOT, which is required as an input in our model of resistivity.

Below are some tables that summarize parameters related to Trinidad U-3 and properties of mud, casing, cement, and formation rock in the system extracted from Altun's dissertation (Altun, 1999).

Well ID	U-3	
TVD Casing	1029	ft
Openhole	30*	ft
Mud weight	8.8	ppg
Pump rate	0.25	bpm

Table 2.1 Basic well and LOT data

Formation Young's Modulus	6.40E+05	psi
Formation Poisson's Ratio	0.3*	
Casing Yound's Modulus	3.0+E7*	psi
Casing Posson's Ratio	0.3*	
Cement Young's Modulus	6.0E+6*	psi
Cement Poisson's Ratio	0.25*	
Compressibility of mud	2.89E-06	(1/psi)
Viscosity of mud	30*	cp

Table 2.2 Properties of mud, casing, cement and formation

*assumed by Fu (2014) in Wider Windows LOT model

As mentioned above, values with asterisk in front are properties reasonably assumed by Fu (2014) in his study of Trinidad U-3 with Wider Windows model. In order to complete the Wider Windows LOT model, some more parameters are needed, which are either extracted by Fu (2014) from Altun (1999) or reasonably assumed to be some value within practical limits.

2.3 Effects on resistivity during LOT

According to Archie's law, true resistivity of a formation depends upon porosity, water saturation, and formation water resistivity. Archie formulated a relationship between true resistivity of the formation, resistivity of water in the formation, porosity, and water saturation (Archie, 1942). Archie's equation has the following form:

$$R_T = \frac{aR_w}{\varphi^m S^n} \tag{2.5}$$

where,

$R_T = True\ formation\ resistivity$

$R_w = Formation\ water\ resistivity$

$\varphi = Porosity$

$S = Water\ saturation$

$a = Tortuosity\ factor$

$n = Saturation\ exponent$

$m = Cementation\ exponent$

a, m, and n are constants that depend upon lithology (compaction, pore structure , and grain shape), pore network connectivity, and rock wettability respectively. In our model, a, m, and n are assumed to be 1, 2, and 2 respectively, as it is typically done unless there is a reason to believe otherwise. If a formation is well characterized through log data and lab test on cores, estimated values specific to that particular formation can be used for the constants instead of these generic values.

Archie's equation can be used to determine how true resistivity of the formation changes during LOT. There are two mechanisms through which resistivity of the formation can change during LOT. First is the invasion of drilling fluid into the formation during LOT. Invasion can change water saturation, salinity or both to a certain extent depending on the properties of drilling mud, formation fluid, and formation rock. If drilling fluid has a resistivity considerably different from formation water resistivity, then resistivity in the invaded zone is strongly influenced by mud filtrate's resistivity. As invasion progresses, this change in resistivity should be observed deeper into the formation. Second mechanism that can affect the resistivity of a formation during LOT is deformation and consolidation caused by the increased pressure in the wellbore. Such consolidation can change the porosity of rock around wellbore region, which can directly affect the resistivity of the formation in that region.

2.3 Resistivity tool response and Depth of Investigation (DOI)

Logging-while-drilling (LWD) resistivity-at-bit (RAB) tools can be used to detect the above-mentioned effects on resistivity around wellbore during LOT. These tools may be inserted a few feet behind the bit in the drill string and can provide resistivity measurements at multiple depths of investigation. These tools are designed to withstand

high pressure, so they can easily endure the pump pressure during LOT. RAB tools are, however, not run routinely during LOT. Running a LWD RAB log to get resistivity measurements around wellbore region during LOT can be beneficial to investigate how the drilling mud is invading and deforming the formation. With the use of a computational model that can predict resistivity changes around open hole during LOT, results from the model can be compared with field data to see what set of parameters in the model predict a closer match. This can give important ideas about properties like permeability and compressibility of the formation. This thesis serves as the first stage of work towards such model that can predict resistivity tool response during LOT. As a first step, resistivity change is being modeled at every point in the formation during LOT.

To have an idea of how RAB tool might respond to LOT, an example of RAB tool response in a fractured interval has been shown below.

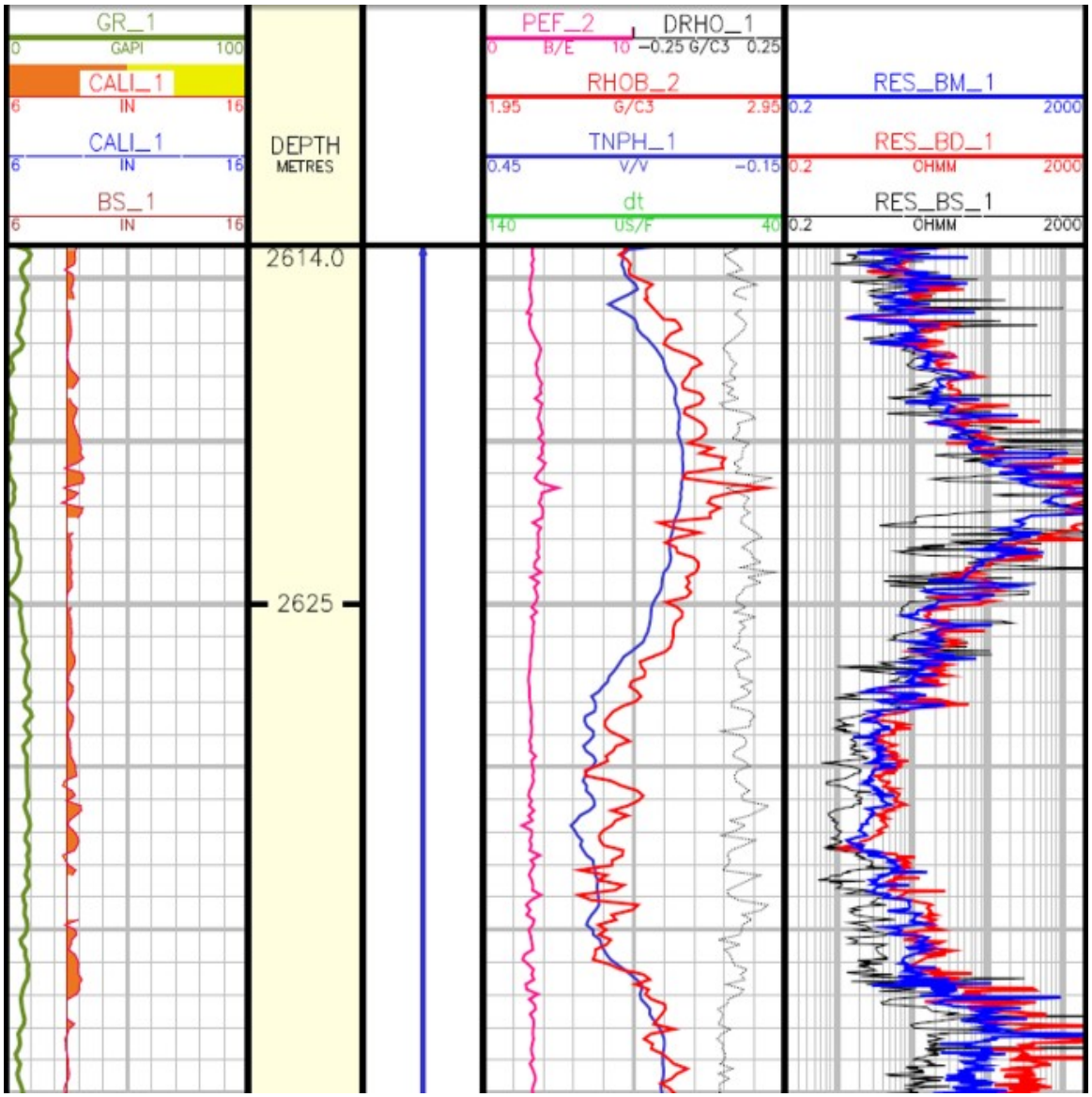

Illustration 2.1 RAB tool response in a fractured reservoir (Crain)

Illustration 2.1 shows a typical log with a number of parameters reported along the depth of the formation. The rightmost column shows RAB tool response in the interval. To understand what different colors represent, the concept of depth of investigation (DOI) must first be understood well. DOI is the radial distance into the

formation starting at the wellbore that a tool penetrates to get its measurement. RAB tools can be made to focus their current shallower or deeper into the formation to alter their DOI through use of their button electrodes mounted on the side of the drill collar. At each depth, RAB tools can make multiple measurements of resistivity by focusing the current only to a certain volume around the wellbore for each measurement. This results in resistivity readings at multiple depths of investigation (Rosthal, Young, Lovell, Buffington, & Arceneaux, 1995). Usually, RAB tools are designed to take three readings at each depth classified as shallow, medium, and deep resistivity. Shallow has the smallest DOI, and deep has the largest DOI.

Getting back to the RAB tool response in the log above in Illustration 2.1, red line in the rightmost column is the deep resistivity response, blue line is the medium, and black line is the shallow response. As the tool enters the zone with fracture, separation between the three lines is observed. The separation is due to the fact that the three responses are not being affected evenly during LOT. As invasion occurs, the shallow response is affected the most, because most of the region that it investigates is being affected due to invasion. This is evident in Fig 2.5 where the black line representing shallow tool response starts to separate at first, and then, the blue representing medium response separates. As the fracture gets bigger with depth, invasion is more severe, and hence the lines move apart more rapidly.

RAB tool response during LOT is conceptually similar to what happens in a fractured interval. Only this time, change in resistivity is measured with respect to time at a specific depth during LOT.

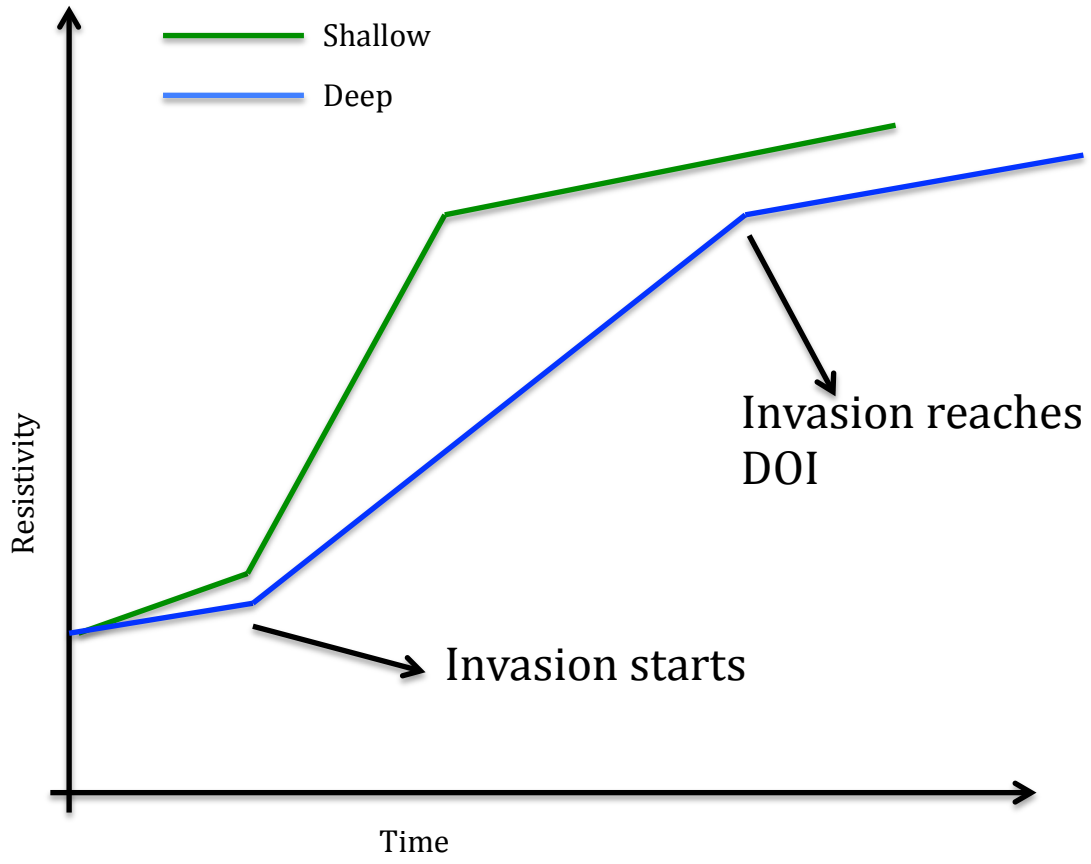

Fig 2.5 Schematic of shallow and deep response during LOT

During LOT, shallow and deep resistivity responses are affected differently as shown above in the schematic. At first, as pump pressure goes up, formation deforms and resistivity changes around the wellbore. Usually, compression results in a decrease in porosity and increase in resistivity near wellbore. Shallow curve is comparatively affected more by deformation, because the effects are stronger near the wellbore, where the shallow tool mainly investigates. After certain time, pressure in the wellbore exceeds leak-off pressure, and invasion starts. Invasion's effect on resistivity is much stronger than deformation's effect, especially if there is a large contrast in mud resistivity and

formation resistivity. Again, shallow tool response is affected first due to invasion. If mud filtrate resistivity is greater than formation water resistivity, the shallow resistivity increases rapidly as soon as invasion starts. After invasion reaches the shallow measurement's DOI, the effects of invasion stabilize, and the shallow curve approaches the resistivity value corresponding to a formation filled with mud filtrate instead of formation water. As invasion advances beyond shallow resistivity DOI, shallow curve now goes up only a little bit with time due to deformation and consolidation, but not as much as due to invasion. Deep curve goes up slowly compared to shallow curve during invasion, resulting in a separation between two responses; however, as invasion front comes closer to the deep resistivity DOI, separation between two responses starts to decay and finally, settles down at a minimum after the invasion front has passed the deep resistivity DOI. This is because the two responses are essentially investigating a similar zone filled with invasion fluid. Yet, some difference remains in shallow and deep tool response even after the invasion radius exceeds deep resistivity DOI because of non-uniform radial deformation during LOT and also because of the fact that with further invasion, saturation profile and concentration profile may change with time. These changes might not be as big as when invasion occurs in the region for the first time, but nevertheless, they are there.

Chapter 3: Approach to model resistivity

Combined effects of deformation and invasion on resistivity during LOT can be investigated by invoking Archie's law at every location in the formation as done by Cozzolino et al (Cozzolino, Howard, & Protazio, 2000). Resistivity at any radial position in the formation at any time during LOT is the function of porosity, water saturation and formation water resistivity. Assuming azimuthal symmetry, which is one of the intrinsic assumptions in our model, resistivity around wellbore at any depth during LOT can be given by the following expression:

$$R(r,t) = \frac{aR_{eq}(r,t)}{\varphi(r,t)^m S(r,t)^n} \tag{3.1}$$

where

$R = True\ formation\ resistivity$

$R_{eq} = Equivalent\ resistivity$

$\varphi = Porosity$

$S = Water\ saturation$

$a = Tortuosity\ factor$

$n = Saturation\ exponent$

$m = Cementation\ exponent$

Note that formation water resistivity term in Archie's equation, R_w has been replaced by equivalent resistivity, R_{eq}. The reason is water resistivity in the formation is no longer constant. Due to invasion during LOT, saturation of water in the formation can change leading to a volumetric mixture of mud filtrate and formation water in the invaded zone. Resistivity of this mixture, R_{eq}, is the volumetric average of resistivity of mud filtrate and formation water at any point in the formation, assuming that the formation

water is not displaced during invasion, and all the additional water saturation at any point comes from mud filtrate invasion and has mud filtrate resistivity. In addition to this, the formation water resistivity changes during LOT due to solute transport of conductive ions, so R_w is no longer constant. It is the resistivity of the initial resident water in the formation that has changed due to diffusion and advection.

$$\frac{1}{R_{eq}(r,t)} = \frac{F_w(r,t)}{R_w(r,t)} + \frac{(1-F_w(r,t))}{R_{mf}} \tag{3.2}$$

$$F_w(r,t) = \frac{S_{wi}}{S_w(r,t)} \tag{3.3}$$

where

$R_{eq} = Equivalent\ resistivity$

$R_w = Formation\ water\ resistivity$

$R_{mf} = Mud\ filtrate\ resistivity$

$S_{wi} = Initial\ water\ saturation\ (constant)$

$S_w = Water\ saturation\ during\ LOT\ (variable)$

In a water-saturated interval, water saturation is constant and is always equal to 1. In that case, Archi's equation simplifies further as shown below in Eq. 3.3.

$$R(r,t) = \frac{aR_{eq}(r,t)}{\varphi(r,t)^m} \tag{3.3}$$

The equivalent resistivity in this case doesn't depend upon saturation; instead, it depends only on the concentration of conductive ions in formation water, which changes with time. Invasion in a water-saturated interval affects the formation water resistivity through dispersion and advection of conductive ions.

In summary, deformation and invasion are the mechanisms through which resistivity around wellbore changes during LOT. In this chapter, the approach developed towards modeling the effects of deformation and invasion during LOT in order to be able to characterize the resistivity change has been discussed.

3.1 Effect of deformation during LOT

Deformation due to pressurized wellbore causes porosity changes around wellbore in the formation. To model the effect of deformation, a simple strain-based porosity model has been used. This porosity model assumes that the grains are incompressible so that volumetric change at any point in the formation is accounted for by change in pore space only. This assumption is practical, as it is obvious that the compressibility of grains is much lower than the compressible of pore spaces filled with pore fluid. If the volumetric strain distribution in the formation can be obtained, a strain-based porosity model can be used to get the effect on porosity during LOT.

$$\epsilon_v = \frac{\Delta V}{V} \tag{3.4}$$

$$\Delta V = \Delta V_p + \Delta V_g \cong \Delta V_p \tag{3.5}$$

where,

$\epsilon_v = Volumetric\ strain$

$\Delta V = Change\ in\ total\ volume$

$\Delta V_p = Change\ in\ pore\ volume$

$\Delta V_g = Change\ in\ grain\ volume$

As it can be seen in Eq. 3.4, negative volumetric strain corresponds to compression, which causes porosity to decrease. Using the definition of volumetric strain to substitute it for change in porosity, the porosity at any point in the formation can be determined by using Eq. 3.8 given below.

$$\Delta\phi = \frac{\Delta V_p}{V} \cong \epsilon_v \tag{3.6}$$

$$\phi = \phi_o + \Delta\phi \tag{3.7}$$

$$\phi(r,t) \cong \phi_o + \epsilon_v(r,t) \tag{3.8}$$

where,

$\epsilon_v = Volumetric\ strain$
$e = Void\ ratio$
$\phi_o = Initial\ porosity\ (constant)$
$\phi = Porosity\ during\ LOT\ (variable)$

It is assumed that initial porosity in the tested open hole interval of the formation is uniform before LOT begins, and as LOT starts affecting the formation around wellbore, porosity changes as a function of volumetric strain. If the volumetric strain at each point in the formation during LOT can be obtained somehow, that information can be used to model the effect of deformation by updating the formation porosity at that point as LOT progresses as shown by Eq. 3.8. In this particaular model, strain distribution is determined using a 3-D Finite Element Method (FEM) model in Abaqus. Next chapter

will be dedicated entirely to the modeling done in Abaqus in order to solve the deformation part of the problem.

3.2 Effect of invasion during LOT

As it is briefly mentioned above, invasion can change the resistivity of the formation by affecting its water saturation and/or salinity. Water salinity is the NaCl content, and it correlates to water resistivity. Some fraction of the conductive ions in drilling mud and formation water might be some other ionic compound than NaCl; however, we express salinity as equivalent NaCl concentration and vice-versa. In this regard, by saying salinity, we are technically referring to the equivalent NaCl concentration.

Depending on the initial water saturation in the formation and the type of mud used for LOT, either saturation change or salinity change can be dominant in contributing towards resistivity change. Sometimes, both can be equally important.

For example, in a fully water-saturated interval, saturation is always 1. As a result, saturation change is not the reason behind resistivity change. In that case, change in formation water resistivity is the primary cause of true formation resistivity change. In an oil-saturated interval however, saturation change is an important parameter. Cleary, resistivity of the formation changes if water saturation increases due to invasion of water-based mud in an oil-saturated interval. The formation water resistivity also changes according to the concentration gradient assuming that diffusion occurs at residual water saturation; however, such effects are expected to be small, because residual water is only a small fraction of total saturation.

It is observed that when the formation is partially water-saturated, the problem is more interesting. On one hand, saturation changes with time, and on the other hand, salinity of the initial formation water can change considerably with time as well due to solute (conductive ions) transport between drilling mud and formation water which is at an arbitrary saturation. The effects of two mechanisms are superposed to come up with a solution. Obviously, both saturation and formation water resistivity will change with time. To calculate the equivalent resistivity using Eq 3.1, the fact that initial formation water doesn't remain at initial salinity, but has its concentration profile change with time, is accounted for in the calculation. As a result, formation water resistivity term in Eq 3.2 is a function of radial distance and time during LOT. How this concentration profile changes with time can be determined under certain assumptions by using the same approach used for fully water-saturated case.

For the purpose of demonstration, the model developed in this work has been used to study the effect of invasion on resistivity during LOT on a fully water-saturated interval, a fully oil-saturated interval, and an interval at an arbitrary initial water saturation respectively. In the fully water-saturated case, salinity change is the only mechanism at work. In the fully oil-saturated case, salinity is less important, and saturation change is what controls formation resistivity, but salinity change in residual water must also be accounted for even though the ultimate effects on true resistivity might be small. Studying the two mechanisms one at a time can be useful to visualize the sole effect of each mechanism separately. At arbitrary initial water saturation, both overall saturation change and salinity change of initial formation water due to dispersion and mixing are relevant, but which of the processes has dominating effect on resistivity change will be determined using our model.

Below, the detailed approach used to model the effect of invasion during LOT in a fully water-saturated interval, a fully oil-saturated interval, and for an intermediate case with arbitrary initial water saturation has been discussed.

3.2.1 Fully water-saturated interval

Most LOT's are performed on water-saturated intervals, so this method has a greater applicability in terms of analyzing field data from such intervals. In a fully water-saturated interval, water saturation stays constant at 1. Primary mechanism that affects the true resistivity of the formation in such scenario is the change in formation water resistivity. Formation water resistivity changes, because concentration of conductive ions in formation water changes with time due to radial solute transport in the formation. Using Eq. 3.9 and 3.10, resistivity of drilling mud and formation water can be converted into equivalent NaCl concentration and vice-versa within an error of approximately 2% when the concentration of NaCl is between 500 and 100,000 ppm (Torres-Verdin, 2013). The problem can then be solved in the form of a time-dependent diffusion-convection problem, which is a very famous problem in ground water contamination and tracer injection experiments.

$$R_w\,(\Omega m) \approx \left(0.0123 + \frac{3647.5}{[\mathrm{NaCl}]^{0.955}}\right) * \left(\frac{81.77}{T\,(°\mathrm{F})+6.77}\right) \tag{3.9}$$

$$[\mathrm{NaCl}]\,(ppm) = 10^{\left\{\frac{3.562-log10\left[\left(\frac{T+6.77}{81.77}\right)R_W-0.0123\right]}{0.955}\right\}} \tag{3.10}$$

In the most general form, the convection-diffusion equation can be written as follows.

$$\frac{\partial C}{\partial t} + \vec{v}.\nabla C = \nabla(\mathrm{D}\nabla C) \tag{3.11}$$

where,

$C = \ Concentration\ gradient$

$v = Interstitial\ flow\ velocity = \dfrac{Q}{2\pi rh\phi}$

$D = Dispersion\ /Diffusion\ coefficient$

The dispersion/ diffusion coefficient (D) represents contributions from molecular diffusion (D_{diff}), mechanical dispersion (D_{mech}), and fluid mixing in the system (D_{mix}). For solute transport, $\mathrm{D}_{diff}\ and\ \mathrm{D}_{mix}$ are generally very small compared to D_{mech} (Fallico, Chidichimo, & Straface, 2012). Contributions from molecular diffusion and fluid mixing have been neglected in our model.

D_{mech} has been well known to vary linearly with fluid velocity (Hiby, 1962; Miller & King, 1966; Poulsen, Suwarnarat, Hostrup, & Kalluri, 2008), so it is expressed as shown below.

$$\mathrm{D}_{mech} = v\alpha_L \tag{3.12}$$

where,

$v = Fluid\ velocity$

$\alpha_L = Longitudinal\ dispersivity\ in\ the\ flowing\ phase\ (constant, L)$

α_L is a property of the porous medium, which is highly scale dependent. Dispersivity measured at laboratory scale is much smaller than that measured at field scale. This scale effect is due to heterogeneities in field scale measurements, which stretch out the concentration profile mimicking larger dispersion (Peters, 2012). Arya et al. (1988) have plotted the dispersitvities of different formation types against the length scale over which they were measured and come up with a relationship for dispersivity on

field scale, which will be used by our model. Length scale in our case is the distance from wellbore to the model boundary, which is about 10 ft.

$$\alpha_L = 0.229L^{0.755}$$

where,

$L = Length\ scale\ of\ measurement$

Combining Eq. 3.9 and Eq. 3.10 with an assumption that mechanical dispersion is the only dominant mechanism of dispersion, it is possible to come up with a radial solute transport equation, which, with appropriate initial and boundary conditions, can be solved to obtain the radial concentration profile with time.

$$\frac{\partial C}{\partial t} = v\alpha_L \frac{\partial^2 C}{\partial r^2} - v\frac{\partial C}{\partial r} \tag{3.13}$$

It has been assumed that the problem is radially symmetrical, which means the formation is homogeneous around wellbore. It is also assumed that the flow rate is uniform in the entire cylindrical open hole, because variation in flow rate with depth in the open hole is negligible, since pressure variation in the open hole is a very small fraction of the actual pressure at that depth. This means that the radial concentration profile is independent of depth, and the same profile extends outward along the entire open hole. Looking at the nature of partial differential equation above, two boundary conditions and an initial condition are needed to fully define and solve this problem.

Chen (1987) has investigated in detail the radial solute transport equation and appropriate boundary conditions involved in this problem. The first boundary condition is the far-field condition, which says that the concentration remains unaffected at a distance far enough from wellbore. The second boundary condition is at the wellbore. We can

either use a Dirichlet boundary condition (first type) or a Cauchy boundary condition (third type) depending on the time scale of our problem. Dirichlet boundary condition assumes the injection well to be a cylindrical source of solute with a constant concentration strength, where as, Cauchy boundary condition invokes mass balance across the wellbore interface to come up with a mixed type boundary condition.

At a distance far away from wellbore:

$$Dirichlet\ BC: \qquad C(r_e, t) = C_f \tag{3.14}$$

At the wellbore radius:

$$Dirichlet\ BC: \qquad C(r_w, t) = C_o \tag{3.15}$$

$$Cauchy\ BC: \qquad QC_o = 2\pi r_w h\phi(vC(r_w, t) - v\alpha_L \frac{\partial C(r_w,t)}{\partial r} \tag{3.16}$$

where,

$r_w = Wellbore\ radius$

$r_e = \ Outer\ boundary\ (typically\ assuemd\ to\ be\ around\ 10 * r_w)$

$C(r_w, t) = Concentration\ at\ the\ wellbore\ radius\ at\ any\ time$

$C_o = Constant\ concentration\ of\ injection\ fluid$

$C_f = Initial\ concentration\ of\ formation\ water$

$h = Height\ of\ injection\ zone$

$\phi = Porosity$

$Q = Leakage\ rate$

Initially, if the concentration in injection fluid is very different from the formation water concentration, a sharp gradient exists across the wellbore interface. This local gradient decreases rapidly with time as more solute mass is transferred across the interface by injection. After a while, concentration at the wellbore radius becomes equal to the concentration of injection fluid, C_o. After this time, the two boundary conditions are practically equivalent to each other (Chen C. S., 1987).

In our model, the local dispersion at r_w is ignored, and the more specific Dirichlet boundary condition is used to generate concentration profiles with time during LOT. Clearly, only the more generic Cauchy boundary condition can capture the initial dispersion across wellbore interface, but during LOT, it is not necessary to investigate this initial dispersion, as the concentration gradient across the wellbore interface goes to zero very rapidly compared to the time scale of LOT.

Below is a dimensionless form of the equation along with proper boundary conditions.

$$\rho \frac{\partial U}{\partial \tau} = \frac{\partial^2 U}{\partial \rho^2} - \frac{\partial U}{\partial \rho}, \qquad \rho > \rho_w, and\ \tau > 0 \tag{3.17}$$

$$U(\rho, 0) = \kappa \tag{3.18}$$

$$U(\rho_e, \tau) = \kappa \tag{3.19}$$

$$U(\rho_w, \tau) = 1 \tag{3.20}$$

where,

$$U = Dimensionless\ concentration = \frac{C}{C_o}$$

$$\rho = Dimensionless\ radial\ distance = \frac{r}{\alpha_L}$$

$$\tau = \ Dimensionless\ time = \frac{Q}{2\pi h \phi {\alpha_L}^2} t$$

$$\kappa = Initial\ dimensionless\ formation\ concentration = \frac{C_f}{C_o}$$

Eq. 3.17 is a very common problem in ground water contamination studies and tracer injection tests. The only major difference is the initial condition. Usually, in a tracer injection experiment, initial concentration of the tracer group in the system is zero, but here, we have a non-zero initial concentration. Another thing to note is the Dirichlet boundary condition that we have adopted here, since we are not investigating the early time local dispersion across wellbore interface. Many other studies prefer Cauchy boundary condition, because it gives a more accurate solution in early time before the concentration gradient across wellbore vanishes, as well as in later time, when it is essentially equivalent to Dirichlet boundary condition.

Several analytical approaches have been taken to get a closed form solution for this convection-diffusion problem in a radial flow field (Tang & Babu, 1979; Hsieh, 1986; Chen C. S., 1987; Chen & Woodside, 1988). Veling (2001) has summarized most of the analytical work done to address this problem mathematically and has come up with his own analytical solution for the convection-diffusion equation with full generality. The closed form solution so obtained is in terms of complex functions, like Airy function and is rather difficult to evaluate even though it provides more accurate results if there is such need. For our purpose, since it is not our concern to obtain an analytical solution, the radial convection-diffusion problem is simply solved using Finite Difference Method (FDM) in MATLAB. The concentration profile so obtained is used to model resistivity change during LOT alongside the effect of deformation.

3.2.2 Fully oil-saturated interval

Even though LOT is not usually performed in an oil-saturated zone, it is of theoretical interest to investigate how resistivity is affected in this case. It is a crucial step towards making our method complete and capable of working on a formation with any arbitrary initial water saturation. Same approach can also be useful in post-analysis of resistivity data if we have drilled through and invaded any oil-saturated zone.

In a fully-oil saturated interval, resistivity of the formation is primarily affected due to saturation change. Formation is initially assumed to be at residual water saturation with a certain initial water salinity or resistivity value. Effect of concentration gradient on initial residual water in the formation is incorporated using the method explained in the previous section. In addition to this, as invasion occurs, water saturation in the formation changes introducing mud filtrate into pore spaces. This change in saturation affects the resistivity directly through Archie's equation. In addition to that, it has an indirect affect on the equivalent resistivity of water at the new saturation. In order to get the total effects on true resistivity, it is sufficient to obtain the water saturation profile in the formation with time during LOT.

The two-phase invasion model developed by Cozzolino et al. has been used to model saturation profiles during LOT (Cozzolino, Howard, & Protazio, 2000). Assuming incompressible fluids and radial Darcy flow, Cozzolino et al. have come up with an expression for the speed with which front of a water saturation travels radially outward in the formation during injection, as shown by Eq. 3.21.

$$\frac{dr}{dt} = \frac{Q_o(t) r_w f'_w(S)}{\phi r} \tag{3.21}$$

where,

$Q_o(t) = Volumetric\ flow\ rate\ at\ the\ wellbore\ with\ time$

$f_w'(S) = Slope\ of\ the\ fractional\ flow\ curve$

Eq. 3.21 brings a new parameter into the picture, fractional flow of water. Fractional flow of water is defined as the ratio of the flow velocity of water to total flow velocity. It is important to understand how fractional flow is related to saturation in order to understand how saturation profile can be characterized during LOT using this method. It can already be seen that fractional flow curves are crucial to determine the speed of different saturation fronts.

Fractional flow curves represent the formation fluid properties and mud properties. If horizontal flow is assumed, gravity is neglected, and the effects of capillary pressure are ignored, then fractional flow of water can be modeled using endpoint mobility ratio.

$$f_w = \frac{M^o S^{nw}}{M^o S^{n1} + (1-S)^{no}} \tag{3.22}$$

$$S = \frac{S_w - S_{wr}}{1 - S_{wr} - S_{or}} \tag{3.23}$$

$$M^o = \frac{k_{rw}^o \mu_o}{k_{rw}^o \mu_w} \tag{3.24}$$

$$k_{rw} = k_{rw}^o S^{nw} \tag{3.25}$$

$$k_{ro} = k_{ro}^o (1-S)^{no} \tag{3.26}$$

where,

$f_w = fractional\ flow\ of\ water$

$S = Normalized\ water\ saturation$

$S_w = Water\ saturation$

$S_{wr} = Residual\ water\ saturation$

$S_{wr} = Residual\ water\ saturation$

$M^o = Endpoint\ mobility\ ratio$

$k_{rw}^o = Endpoint\ water\ relative\ permebality$

$k_{ro}^o = Endpoint\ oil\ relative\ permebality$

$nw, and\ no = Exponents\ (constant)$

nw and no are the saturation exponents in water and oil relative permeability equations. These exponents depend on rock properties and can be estimated more accurately for a particular rock formation by running relative permeability experiments on cores. Nevertheless, they come out to be close to 2. Due to the overall effects of viscous fingering and heterogeneity in saturation, it is sometimes suggested that relative permeability has linear relationship with water saturation on field scale (Koval, 1963). In such case, both exponents would be equal to 1. In our model, the value of those exponents can be changed as desired. Unless there is a reason to believe otherwise, the exponents are by default taken to be equal to 2. Similarly, k_{rw}^o and k_{ro}^o are endpoint relative permeabilities of water and oil that are also dependent on rock type. In our model, water and oil endpoint permeabilities are assigned to be 0.4 and 0.8 respectively by default; these are typical values for water-wet rocks.

Eq. 3.22 expresses water fractional flow in terms of water saturation, endpoint mobility ratio, and a few exponents that empirically equate relative permeability with water saturation. Since gravity and capillary effects are ignored, Eq. 3.22 turns out to have a very simple form.

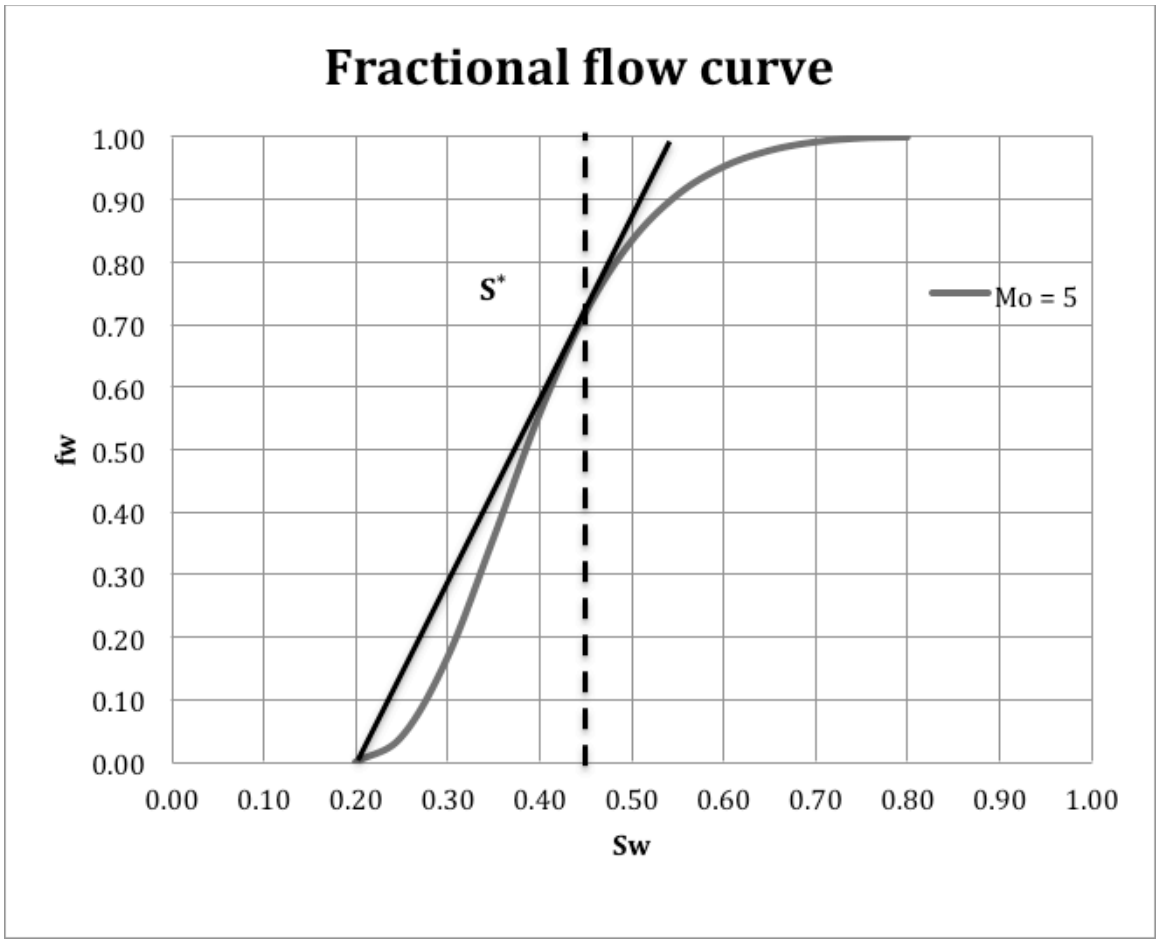

Fig 3.1 Fractional flow curve

Fig 3.1 shows an example of a fraction flow curve with an arbitrarily selected endpoint mobility ratio of 5. The most interesting feature of fractional flow curve is the saturation shock. During invasion, each saturation front travels into the formation at a certain speed that can be determined by using Eq. 3.21. However, one important physical restriction must be applied. If water saturation at the wellbore is higher compared to the

formation being invaded, lowest value of water saturation front must travel farthest into the formation. This means the speed of saturation front must decrease with increasing saturation for an injection at higher water saturation.

Speed of a saturation front is the slope of fractional flow curve at that saturation. In Fig 3.1, let's assume we are injecting at $S_w = 0.8$ into a formation where $S_w = 0.2$. According to the fractional flow curve, the slope goes up first with increasing saturation and then goes down. This is physically impossible, because a higher saturation can't travel farther into the formation than a lower saturation for this case. Hence, there has to be a saturation shock, which is an abrupt change in saturation at some saturation value after which the slope starts decreasing. In the figure above, the shock is at $S_w = 0.45$.

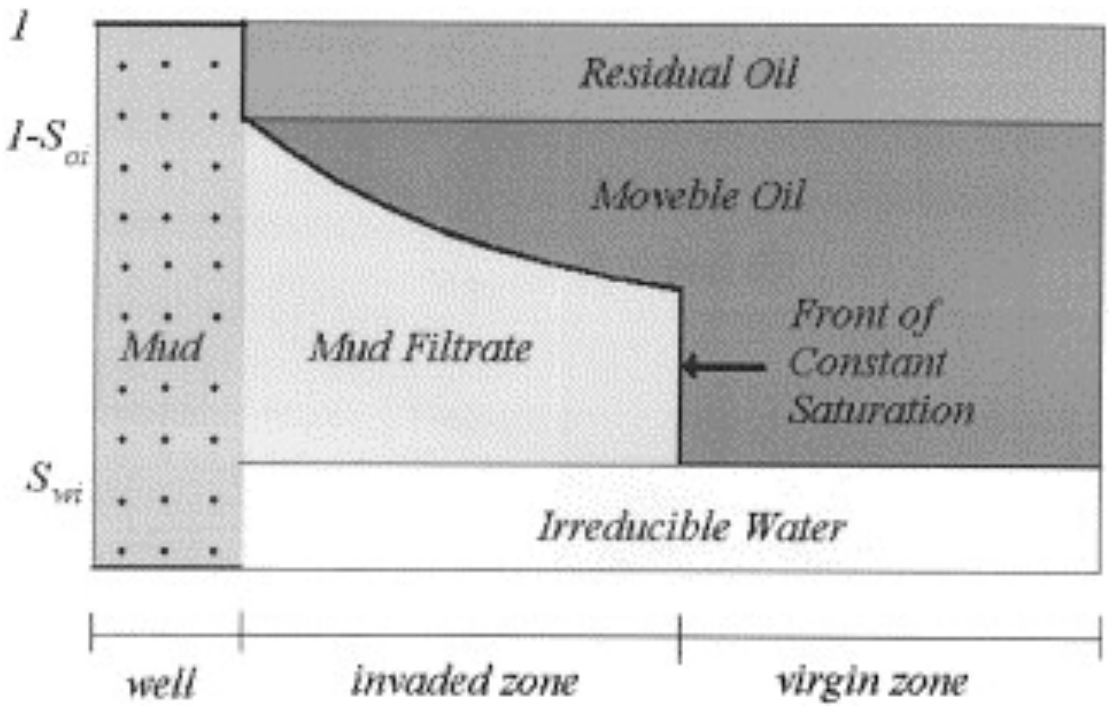

Fig 3.2 Saturation profile during invasion (Cozzolino, Howard, & Protazio, 2000)

Fig 3.2 shows a typical saturation profile during invasion of water-based mud into oil-saturated formation. At the wellbore, water saturation is 1. Going radially outward, water saturation goes down monotonously, but at a certain distance from the wellbore, there is an abrupt change in saturation known as the saturation shock. Beyond this radius, formation is at initial residual water saturation. This is how saturation shock propagates into the formation.

To determine the saturation value at the shock front, material balance can be invoked on two sides of shock saturation, shown in Fig 3.3 by the enclosed areas on two sides of the shock.

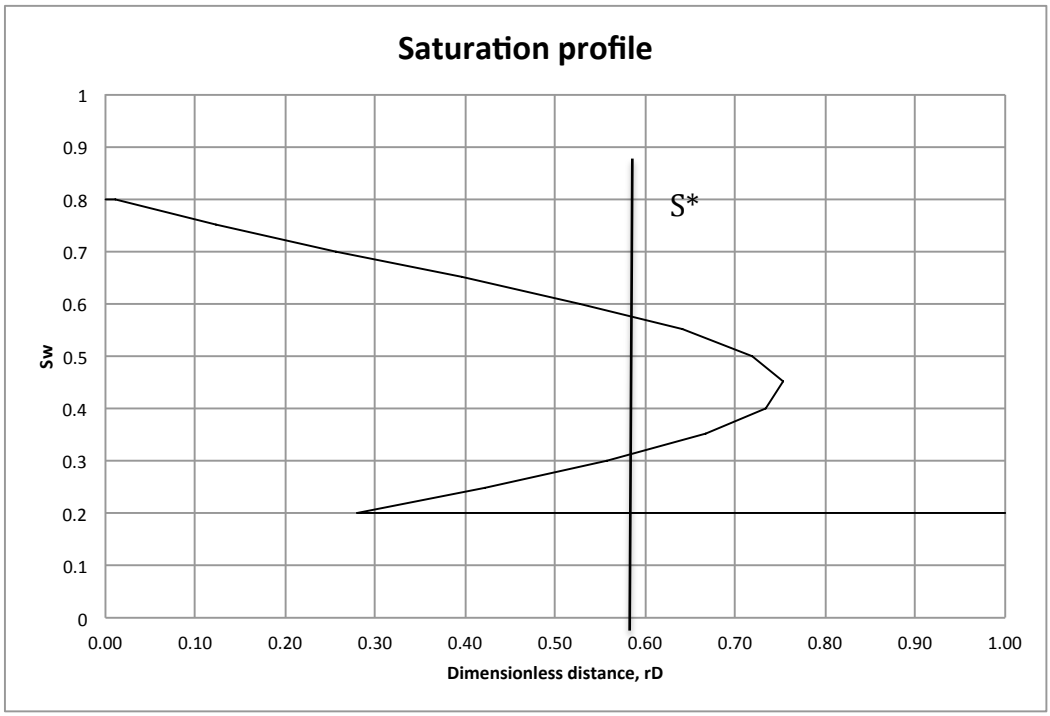

Fig 3.3 Determining shock saturation using mass balance

Using the material balance, it is also possible to analytically come up with an expression to determine shock.

$$\frac{f_w(S^*) - f_w(S_{wi})}{S^* - S_{wi}} = f_w{}'(S^*) \tag{3.27}$$

where,

$S^* = \ Shock\ saturation$

Once radial water saturation profile is obtained, it can be used to investigate how resistivity is changing around wellbore during LOT. Obviously, abrupt change in saturation at the shock translates to an abrupt change in resistivity around wellbore. This will be seen in the results predicted by our model in the coming chapters.

3.2.3 Interval at an arbitrary initial water saturation

If formation water is initially at arbitrary water saturation greater than residual water saturation, it becomes important to study the effects of both saturation change and salinity change to find out which has a dominating effect. Salinity change and saturation change can be investigated using the approaches explained in the previous two sections. This scenario is, in fact, not different from the oil-saturated with diffusion in residual water saturation included; only this time, effects of diffusion and dispersion are more pronounced, since initial water saturation is higher than residual water saturation.

Chapter 4: Implementation in ABAQUS

ABAQUS is a software platform to solve engineering problems using Finite Element Method (FEM). In our research, ABAQUS has been used to solve for the volumetric strain distribution in a given stress field. This accounts for the effect of deformation during LOT. In this chapter, it is explained in detail how this is achieved in ABAQUS.

4.1 Basic model description and specifications

To get the volumetric strain distribution in the formation during LOT, we use a 3-D model in ABAQUS. Casing, cement, and formation rock are all modeled as homogeneous linearly elastic materials with defined values of Young's modulus and Poisson's ratio. This assumption might be valid for the steel casing and the cement around the casing to an extent, but formation rock is certainly a heterogeneous and non-linearly elastic system. The model in its current form does not capture these spatial heterogeneities and non-linear elastic behavior. Modeling heterogeneities in the form of pre-existing fractures and including plastic rock failure around wellbore during LOT are ways these phenomena can be included in the model in future.

Vertically, the model can be divided into three sections as illustrated by Illustration 4.1 in next page. Uppermost section of the model is a 15 ft long interval with casing and cement included around borehole. Next 30 ft section is an open hole section with no casing. This is the interval where LOT is carried out. Final bottom section is a 5 ft deep platform below open hole to allow us to capture any effects of deformation directly below the bottomhole. Laterally, the model is 20'X20' with wellbore at the center.

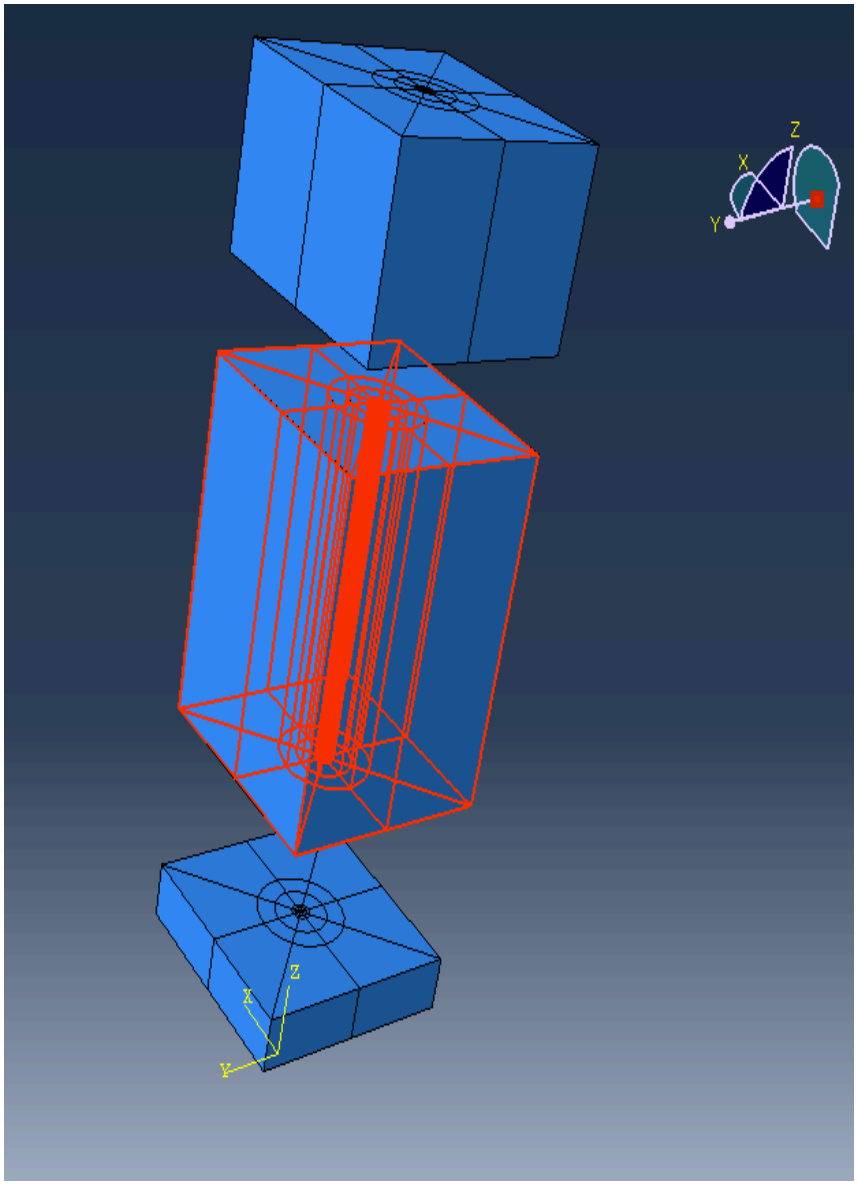

15 ft section with casing and cement

30 ft open-hole section

5 ft platform at the bottom

Illustration 4.1 Modeling in ABAQUS

	Oilfield Units		SI Units	
Casing Inner Radius	8.5	in	0.216	m
Casing Outer Radius	10	in	0.254	m
Cement Inner Radius	10	in	0.254	m
Cement Outer Radius	11	in	0.279	m
Openhole Radius	10	in	0.254	m

Table 4.1 Size of wellbore, casing, and cement sheath

Table 4.1 lists the inner and outer radii of casing and cement sheath and radius of the open hole below the cased interval in oilfield units and SI units. While modeling the system in ABAQUS, SI units are used for convenience and consistency. Since Trinidad U-3 from Altun's dissertation is used for LOT data for a case study in our resistivity modeling, casing outer diameter is set at 20 inches to be consistent with available data for Trinidad U-3. Cement sheath is assumed to be present right outside the casing, and its thickness is assumed to be 1 inch. Since there is no casing or cement present in the open hole, open hole radius is assumed to be 10 inches, which is the outer radius of casing in the previous cased interval.

While solving for volumetric strain distribution in the formation, it is not necessary to solve the full model. By making use of symmetry, the problem can be set up as one quarter of the model with appropriate boundary conditions and the strain distribution can be obtained in the whole region around wellbore. This saves significant computational effort and time. Fig 4.2 shows the quarter model that is actually set up and solved using FEM in ABAQUS.

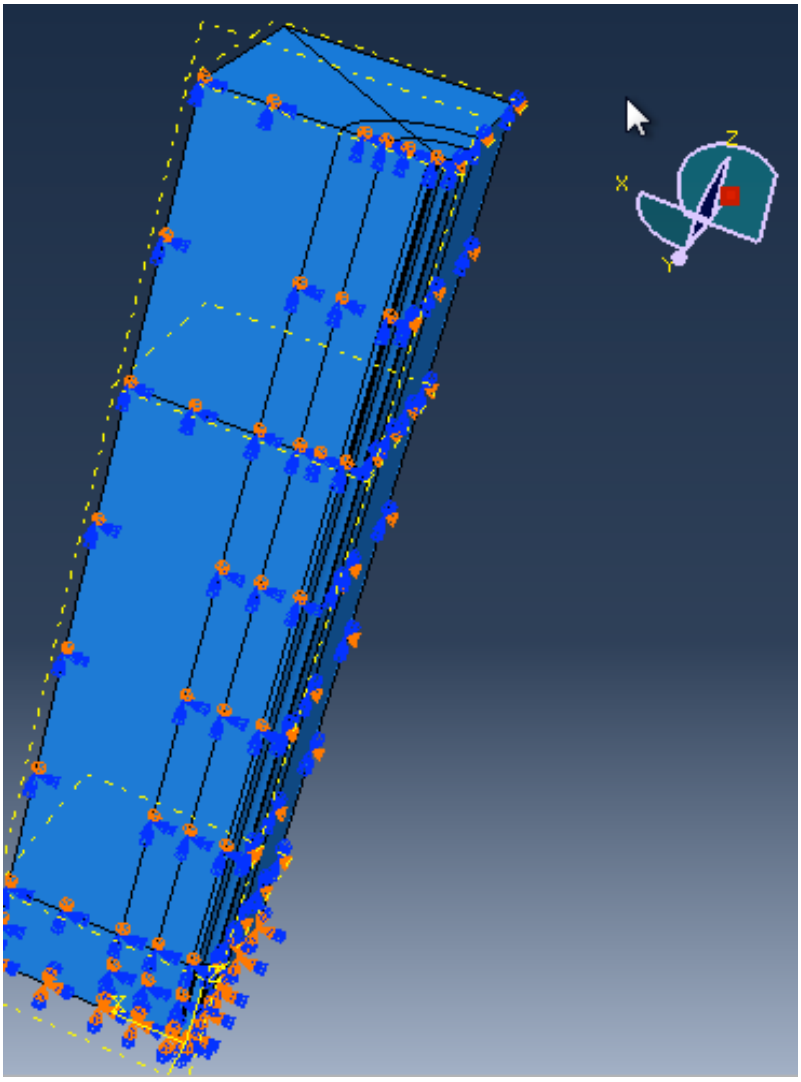

Illustration 4.2 Quarter model to be actually solved using FEM

4.2 Input parameters

There are three parameters required for each material in order to characterize the mechanical behavior of the system under specified stress fields: Young's modulus, Poisson's ratio, and density. Young's modulus and Poisson's ratio dictate how the system deforms under a given stress field. Density is important in order to include gravity in the system and to calculate the overburden stress, which is applied as a boundary condition.

	Oilfield Units		SI Units	
Formation Young's modulus	6.400E+05	psi	4.413E+09	Pa
Formation Poisson's ratio	0.30		0.30	
Formation bulk density	-		2300	kg/m^3
Casing Young's modulus	3.000E+07	psi	2.068E+11	Pa
Casing Poisson's ratio	0.30		0.30	
Casing density	-		8050	kg/m^3
Cement Young's modulus	6.000E+06	psi	4.137E+10	Pa
Cement Poisson's ratio	0.25		0.25	
Cement density	12.0	lbs/gal	1440	kg/m^3

Table 4.2 Properties of casing, cement, and formation rock

Properties in Table 4.2 are consistent with Trinidad U-3. Any property that is missing for the well has been assumed within practical limits.

4.3 Mesh and element type

As it is mentioned in the previous section, it is easier take advantage of the symmetry of our problem and solve for only one quarter of the entire model to get the required results. Illustration 4.3 shows how the quarter model is meshed in ABAQUS.

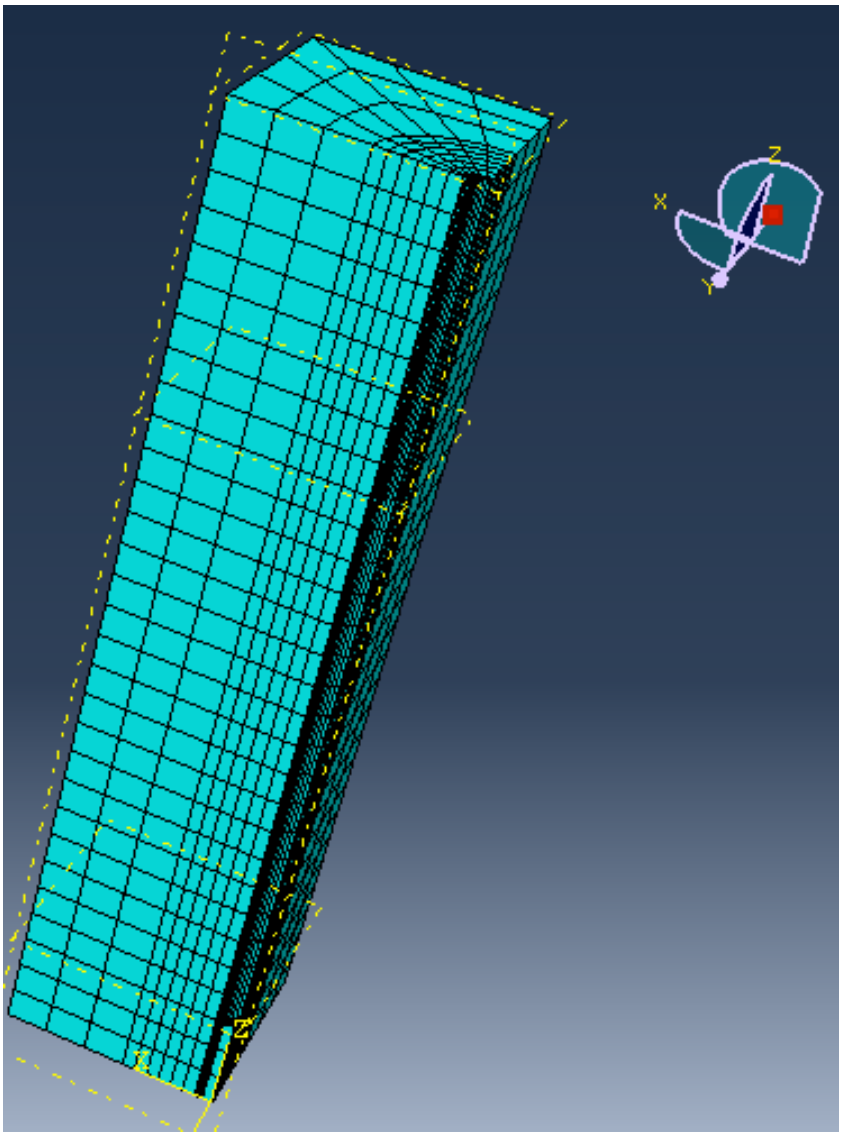

Illustration 4.3 Mesh

Meshing is a very crucial step while setting up any engineering problem using FEM. The type and structure of mesh used can greatly affect the final result. A uniform mesh produces much better result than a non-uniform mesh; that's why our model is meshed in as much uniform fashion as possible by using sweeping technique in ABAQUS. To avoid unnecessary computation, finer mesh is used close to wellbore, where deformation effects are stronger, and coarser mesh is used away from wellbore, as shown in Illustration 4.3. This reduces the number of elements in the model by making the elements that are farther away from wellbore larger in size, which makes the problem computationally less demanding. A mesh analysis is also conducted to find the appropriate element size that can produce the required results most efficiently with good enough accuracy.

Standard 8-node C3D8R elements of linear order that belong to the family '3D Stress' are used while meshing the model.

4.4 Boundary conditions and loads

Proper boundary conditions and loading conditions are needed in order to complete the model definition in ABAQUS. These include vertical overburden and horizontal stresses, symmetry boundary condition on sides adjacent to wellbore, fixed boundary at the bottom, and wellbore pressure at the wellbore interface. Each of these is discussed in this section.

4.4.1 Vertical overburden stress

Vertical overburden stress acts on the upper surface of the model due to the overlying mass.

$$\sigma_v = \rho_m g h \tag{4.1}$$

where,

$\rho_m = Density\ of\ the\ overlying\ material$

$g = Accelaration\ due\ to\ gravity$

$h = Height\ to\ the\ reference\ point$

$\sigma_v = Overburden\ due\ to\ the\ overlying\ mass$

Our model includes cement, casing, and formation rock, which have different densities, so overburden due to these different materials must be different as Eq. 4.1 shows. Using the depth to the top of the model and density of the overlying material, we can compute the overburden for each material and apply it to the appropriate region of the top surface as a boundary condition. Table 4.3 lists the overburden on top of casing, cement, and formation rock due to respective overlying mass. Depth to the top of the model is set equal to Total Vertical Depth (TVD) of Trinidad U-3 minus the cased and open hole interval included in the model, which is 45 ft in total.

	Oilfield Units		SI Units	
Formation overburden	1.025E+03	psi	7.069E+06	Pa
Casing overburden	3.589E+03	psi	2.474E+07	Pa
Cement overburden	6.418E+02	psi	4.425E+06	Pa

Table 4.3 Overburden stress on casing, cement, and formation

4.4.2 Horizontal stress

Horizontal stress acts on the two outer surfaces of the model. Our system is assumed to be transversely isotropic, so horizontal stress is the same in every direction. Even though this is common practice in studying wellbore stresses, in reality, this is unlikely to be the case; in actual rock formations, there is usually some anisotropy in lateral stress fields with different minimum and maximum horizontal stresses acting perpendicular to each other. In this study, the estimated value of minimum horizontal stress is used in all directions to make the formation laterally isotopic. In other words, the anisotropy ratio, which is the ratio of maximum to minimum horizontal stress, is set to 1.

Minimum horizontal stress can be estimated from vertical stress and pore pressure using below given equations.

$$\sigma_{v,eff} = \left(\sigma_v - \alpha P_p\right) \tag{4.2}$$

$$\sigma_{h,eff} = \left(\sigma_h - \alpha P_p\right) \tag{4.3}$$

$$\sigma_{h,eff} = \frac{\nu}{1-\nu}\,\sigma_{v,eff} \tag{4.4}$$

$$\sigma_h \cong \frac{\nu}{1-\nu}\left(\sigma_v - \alpha P_p\right) + \alpha P_p \tag{4.5}$$

where,

$\sigma_{h,eff} = Effective\ horizontal\ stress$

$\sigma_{v,eff} = Effective\ vertical\ overburden\ stress$

$\sigma_h = Total\ horizontal\ stress$

$\sigma_h = Total\ vertical\ stress$

$P_p = Pore\ pressure$

$\alpha = \ Biot's\ coefficient$

Eq. 4.5 relates horizontal stress with effective vertical stress and pore pressure. Overburden can be determined using Eq. 4.1, and pore pressure can be estimated as the bottomhole pressure due to hydrostatic head of drilling fluid before LOT begins. The

constant, Biot's effective stress coefficient, is the ratio of pore-space deformation to total bulk volume change (Biot & Willis., 1957) and is crucial to calculating the effective stress from total stress and pore pressure. Biot's coefficient accounts for the partial reduction in the supporting behavior of pore fluid under compaction, so it generally decreases with decreasing porosity showing it is harder for fluid to move around in smaller space. Cheng's relation for isotropic rock relates Biot's coefficient with bulk moduli of formation rock and solid grain, as shown by Eq. 4.6 below (Cheng, 1997).

$$\alpha = 1 - \frac{K_r}{K_g} \tag{4.6}$$

where,

$K_r = Bulk\ modulus\ of\ rock$

$K_g = Bulk\ modulus\ of\ grain$

Traditionally, Biot's coefficient is obtained in lab by using various experimental methods to get the rock and grain compressibility. One of the most famous methods uses tri-axial compression measurement done on rock samples under constant volumetric strain condition. Since lab tests can be long and expensive, some alternatives have been developed in the form of empirical relationships to obtain Biot's coefficient from porosity for unconsolidated (Lee M. W., 2002) and consolidated sediments (Bailin, 2001). Recently, Luo et al. have come up with a method to estimate Biot's coefficient from well logs (Luo, Were, Liu, & Hou, 2015). For our purpose, Bailin's empirical formula for consolidated sediments that estimates static Biot's coefficient from porosity by using Eq. 4.7 is used.

$$\alpha = \ 1 - exp(-0.038\phi - 0.86) \tag{4.7}$$

where,

$\phi\ (porosity)\ is\ in\ \%$

A rather interesting approach to estimate minimum horizontal far-field stress would be to use LOT data. Gandomkar has suggested an iterative approach to estimate the minimum far-field horizontal stress using LOT data starting with an arbitrary initial estimation (Gandomkar, Fu, & Gray, 2015). This approach can be used in future to estimate minimum horizontal stress. In such case, anisotropy ratio is also needed in order to determine the maximum horizontal stress.

In our model, the average of horizontal stresses at the top and bottom of the model is taken and applied uniformly on the outer surfaces. Since the model height is very less compared to TVD, variation of horizontal stress with depth in the model is minute and negligible.

4.4.3 Symmetry boundary condition

Symmetry boundary condition is applied to the two sides adjacent to wellbore. Symmetry boundary condition means there are no displacements in the direction perpendicular to the plane of the surface and no rotation around that plane. By imposing this condition on the two adjacent faces, the quarter model is essentially mimicking the physical behavior of the full model using a quarter model.

4.4.4 Fixed bottom surface

Surface at the bottom of the 5 ft deep platform is fixed allowing no displacement and no rotation. It is implicitly assumed that the effects of wellbore pressure during LOT are negligible at this distance below the bottomhole.

4.4.5 Wellbore pressure

Wellbore pressure is applied on the surface of wellbore along the cased and open hole interval. As LOT progresses, pump pressure goes up and so does the wellbore pressure. Fig 4.1 shows the plot with digitized LOT data from Fu's thesis for Trinidad U-3. Table 4.4 summarizes the Wider Windows LOT model's leak volume data for Trinidad U-3 extracted from Fu's thesis (Fu, 2014).

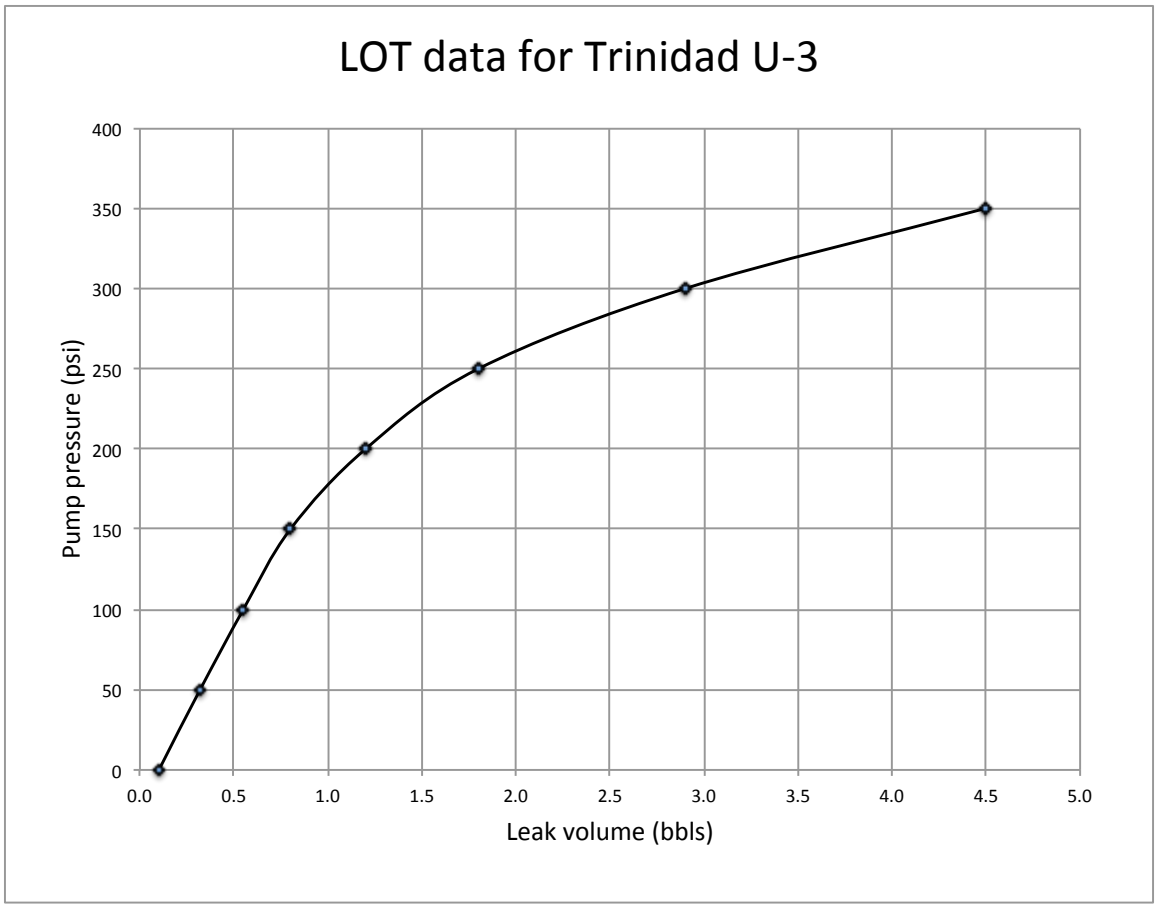

Fig 4.1 LOT data for Trinidad U-3

Fig 4.1 pLOT's pump pressure in y-axis versus leak volume obtained using Wider Windows LOT model in x-axis.

Pump Pressure(psi)	Bottomhole pressure(psi)	Leak volume(bbls)	time(mins)
0	481.36	0.1	0.4
50	531.36	0.3	1.28
100	581.36	0.6	2.2
150	631.36	0.8	3.2
200	681.36	1.2	4.8
250	731.36	1.8	7.2
300	781.36	2.9	11.6
350	831.36	4.5	18

Table 4.4 Wider Windows LOT model data extracted from Fu's thesis for Trinidad U-3

In order to see how deformation occurs as pump pressure goes up, we pick a few pressure points from LOT data and apply the wellbore pressure corresponding to that pump pressure to the wellbore surface in the model. This is done in steps in ABAQUS. After each step, wellbore pressure is updated to a higher value corresponding to the next step. Each step is solved as a static stress-strain problem to get the volumetric strain distribution in the formation at that point during LOT.

4.4 Output in ABAQUS

Once model definition is complete, the model is run in ABAQUS to get the output in the form of strain distribution. If the principal strains in all three directions can be obtained, they can be summed up to get the volumetric strain. Below is a figure that visually illustrates the result obtained in ABAQUS.

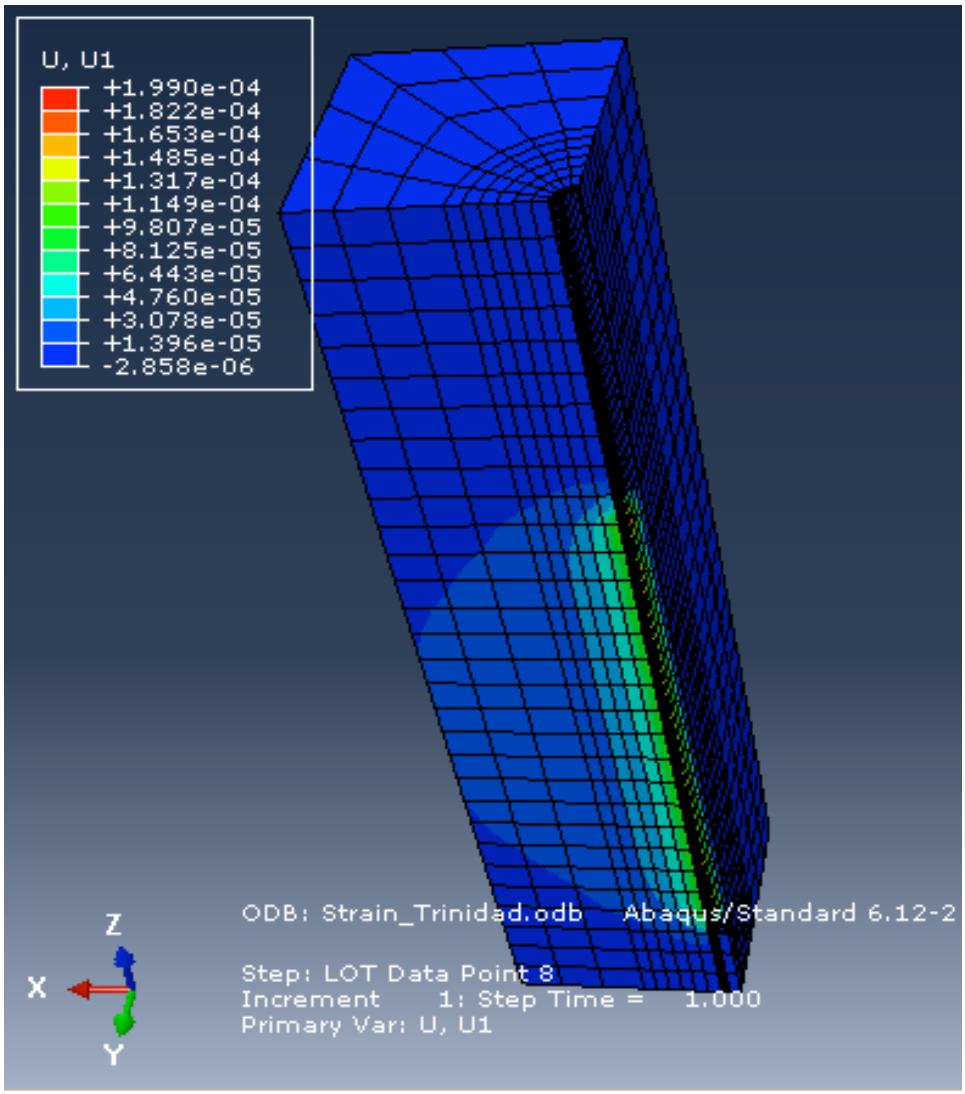

Illustration 4.4 First principal strain output in ABAQUS

Using Python scripts in ABAQUS, volumetric strain distribution can be extracted at any radial distance and depth at any of the steps during LOT. Once the strain data is extracted, porosity change can be computed during LOT using the method discussed in Section 3.1. Formation water saturation and equivalent resistivity can be determined at any radial distance during LOT by using the approach discussed in Section 3.2. Finally, all these parameters can together be used to determine the true formation resistivity at any point in the formation at the time intervals picked from the LOT plot. Results so obtained are compiled in the next chapter.

Chapter 5: Results and Discussion

In this section, radial resistivity profiles of the formation are plotted with time during LOT for Trinidad U-3. Volumetric strain and saturation and/or concentration profiles are obtained using LOT and other data either available or assumed under certain practical assumptions using the approach discussed in Chapter 3 and 4. Radial resistivity profiles are plotted starting at the wellbore radius for an arbitrarily picked depth, in this case, 25 ft below the bottom of the casing. Effects of deformation and invasion (into a fully water-saturated formation and a fully oil-saturated formation) are discussed separately at first, and then, the two effects are combined to investigate the true formation resistivity change around wellbore during LOT. Mud resistivity and initial formation water resistivity are assumed to be 0.25 Ohm-m and 0.5 Ohm-m respectively.

5.1 Deformation

Volumetric strain is obtained as an output from the model developed in ABAQUS to investigate deformation. Strain data is useful while factoring in porosity change while calculating resistivity. Below are the pLOT's of strain in different directions for Trinidad U-3 as LOT progresses.

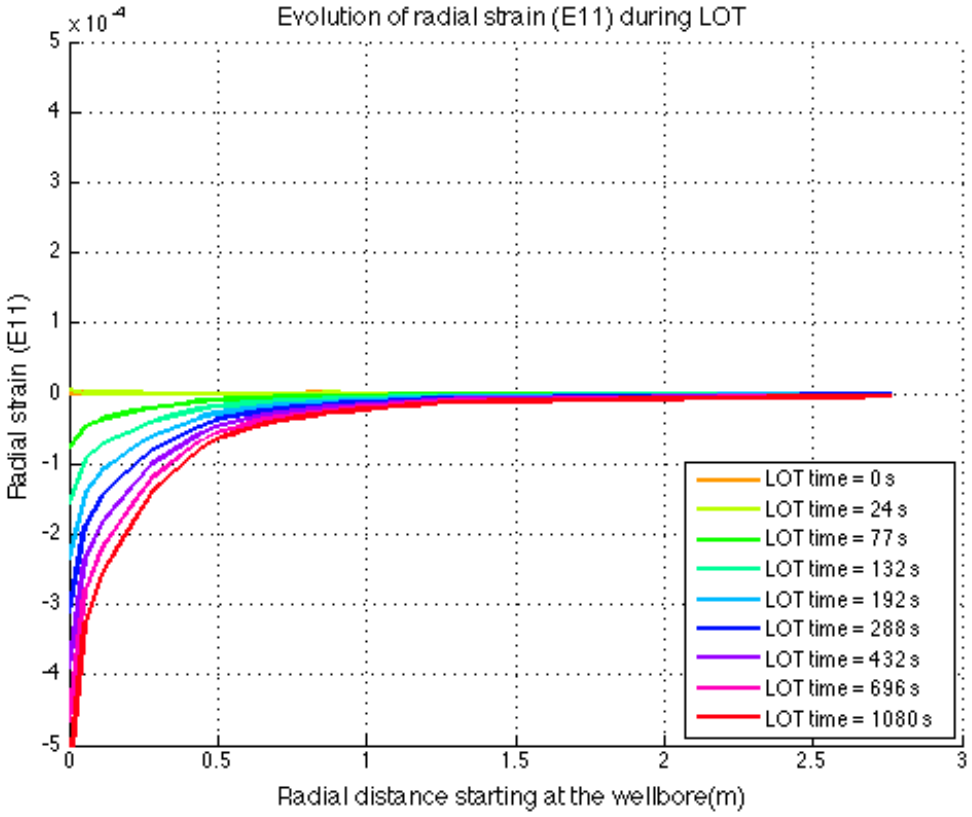

Fig 5.1 Radial strain during LOT starting at the wellbore for Trinidad U-3

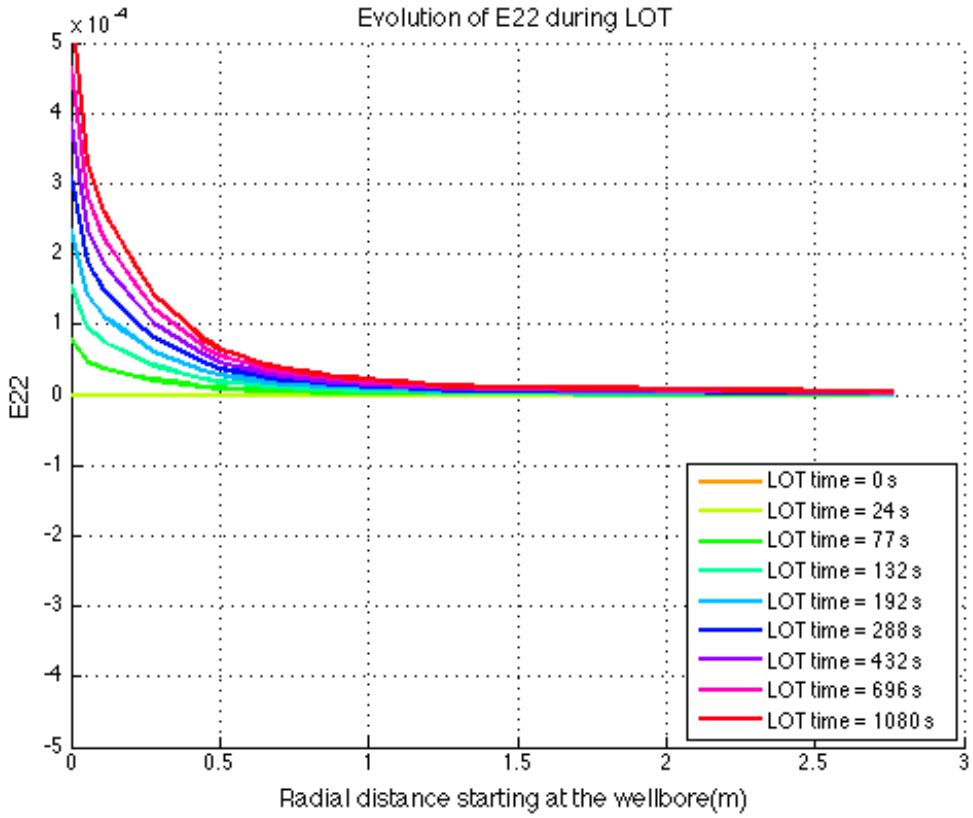

Fig 5.2 Theta strain during LOT starting at the wellbore for Trinidad U-3

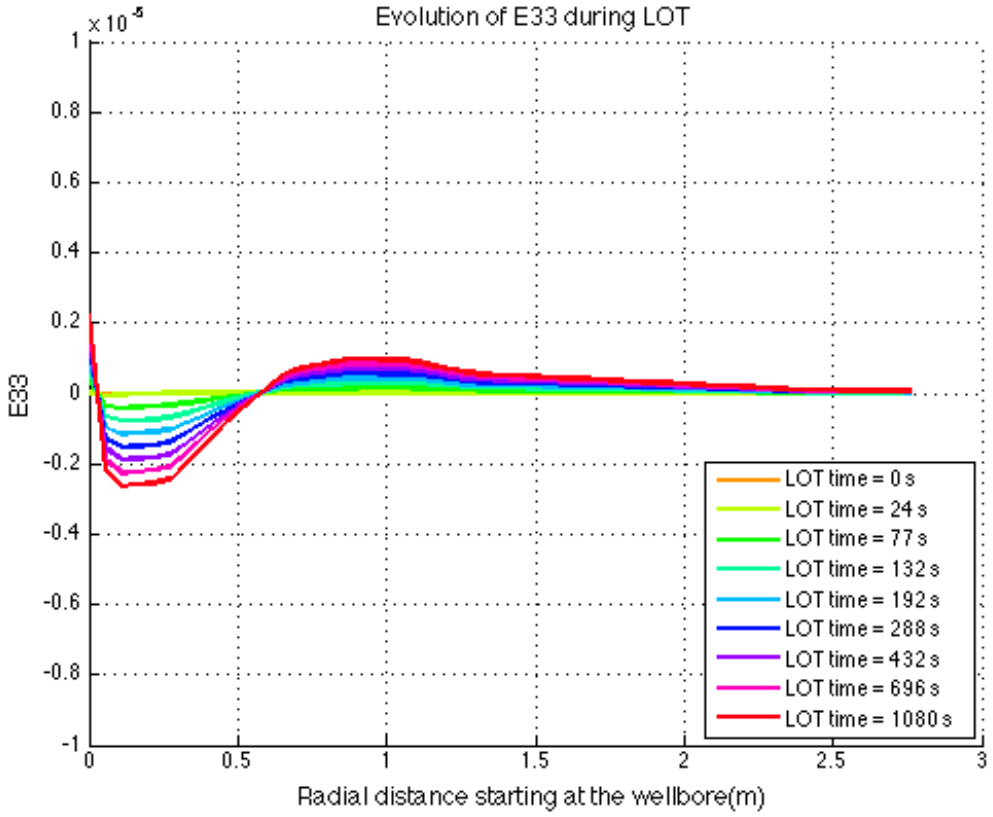

Fig 5.3 Vertical strain during LOT starting at the wellbore for Trinidad U-3

Volumetric strain is the sum of the individual strains in three principal directions. Next, we show a plot of evolution of volumetric strain with time during LOT.

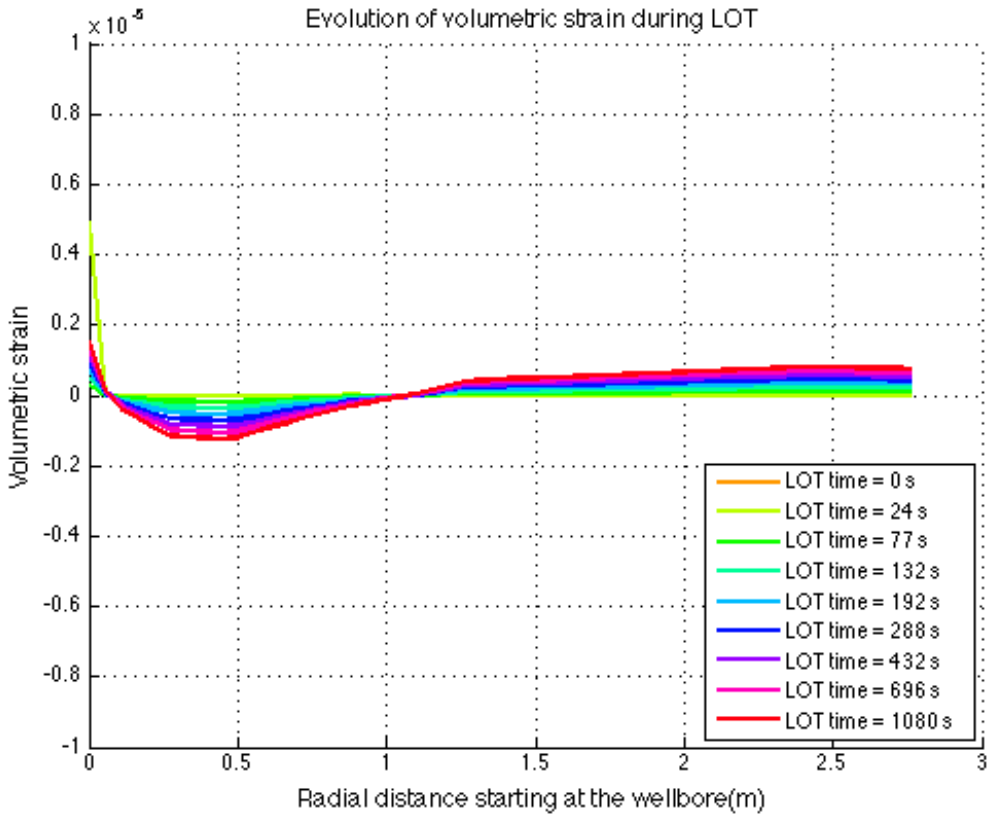

Fig 5.4 Volumetric strain (that is, $\epsilon_{11} + \epsilon_{22} + \epsilon_{33}$) during LOT starting at the wellbore for Trinidad U-3

Once the volumetric strain is obtained, change in porosity in the formation can be determined by using the consolidation model discussed in Chapter 3. Porosity change during LOT is not huge as shown by Fig 5.5 below. It has been mentioned before that the effects of deformation are not as severe as the effects of invasion when it comes to resistivity change around wellbore during LOT.

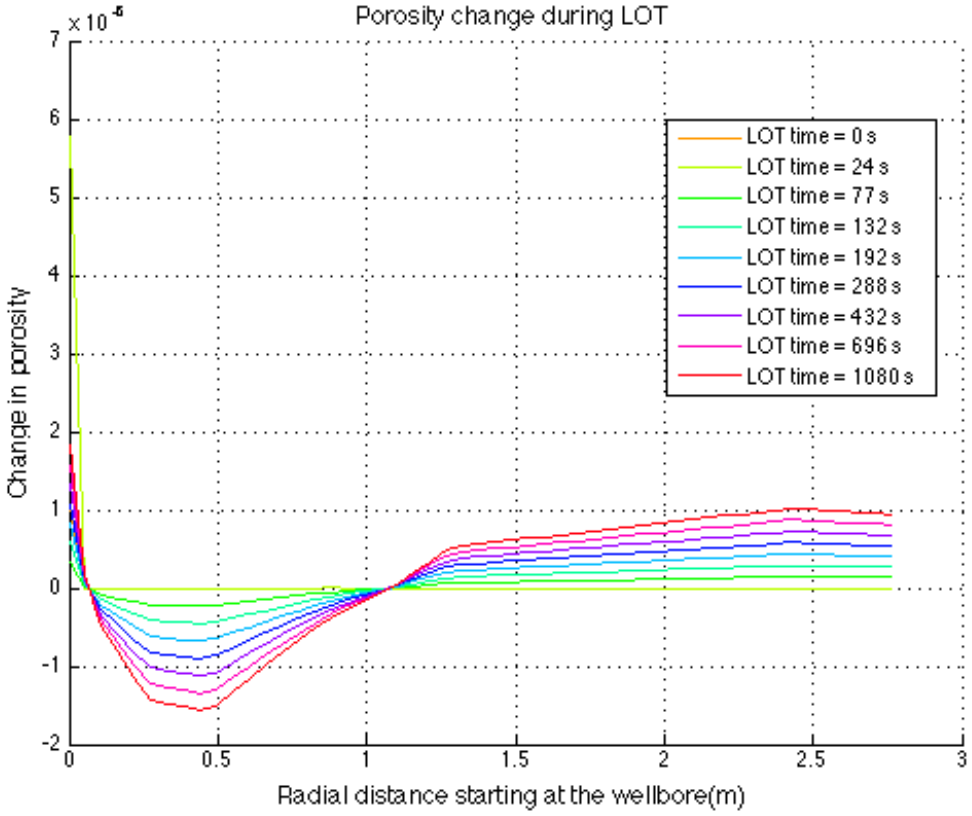

Fig 5.5 Porosity change in the formation radially outward in Trinidad U-3 as LOT progresses

5.2 Invasion

Invasion affects the true resistivity either by changing water saturation or equivalent water resistivity. In this section, three different scenarios; a water-saturated interval, an oil-saturated interval, and an interval with arbitrary water saturation, have

been modeled to see how saturation and concentration profiles affect resistivity during LOT.

5.2.1 Water-saturated interval ($S_w = 1$)

In water–saturated interval, water saturation remains constant at 1. What affects resistivity is the change in salinity of the formation. By modeling resistivity as a function of equivalent NaCl concentration in formation water, it can be predicted how resistivity is affected by diffusion and advection under the existing concentration gradient. In this section, the evolution profiles of equivalent NaCl concentration during LOT are plotted.

Drilling mud is assumed to be fully water-based, and mud resistivity and formation resistivity are assumed to be 0.25 Ohm-m and 0.5 Ohm-m respectively. These resistivity values can be converted into equivalent NaCl concentration by using Eq 3.10. By imposing initial and boundary conditions for concentration, the 2D diffusion-advection can be solved problem by using the finite differencing approach to get the solution at any radial distance with time. Fig 5.6 shows the result.

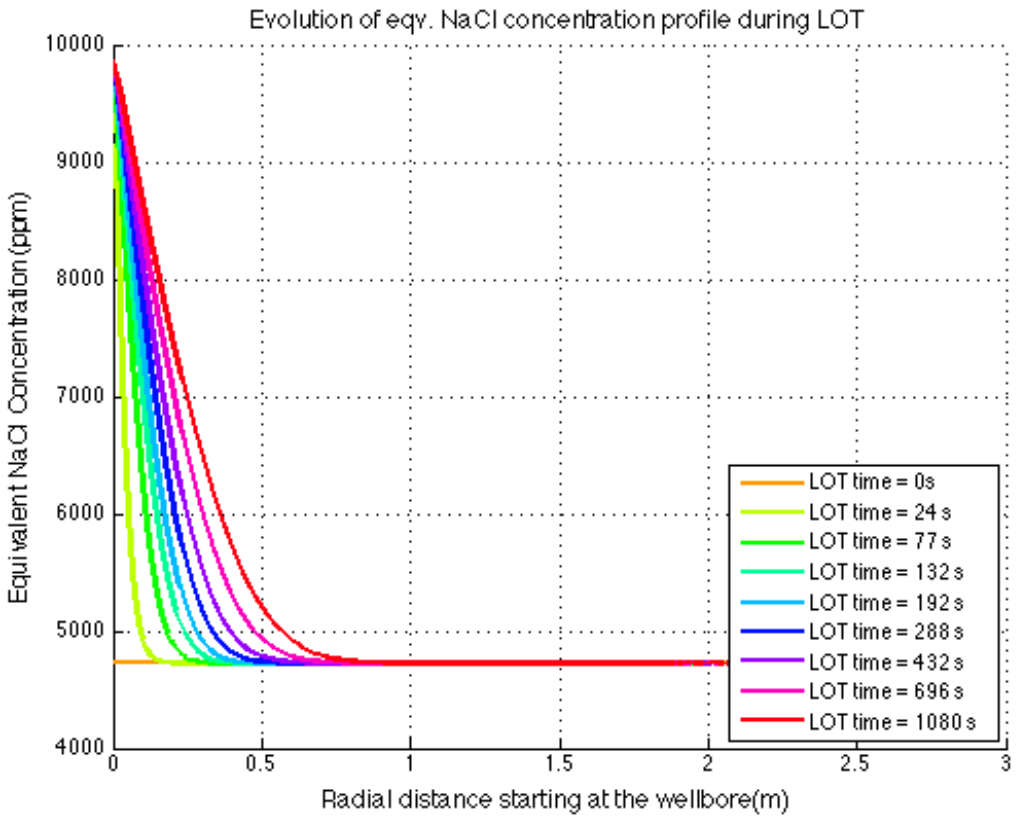

Fig 5.6 Equivalent NaCl concentration profile during LOT

Using Eq. 3.9, equivalent NaCl concentration at any point in the formation during LOT can be converted back into formation water resistivity value at that point. Since salinity increases the conductivity of a solution, equivalent NaCl concentration is related inversely to water resistivity. This is depicted by Fig 5.7, which shows an inverted profile for water resistivity when compared to the concentration profile.

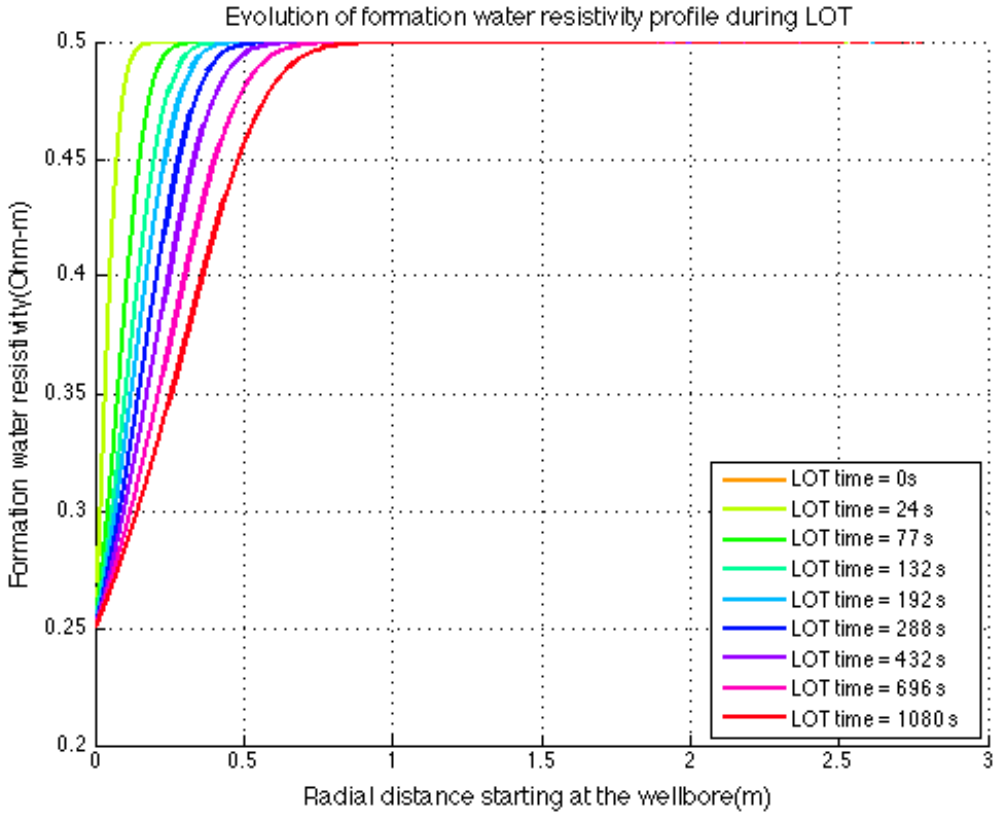

Fig 5.7 Formation water resistivity profile during LOT

Note that formation water resistivity ranges between mud resistivity and initial formation water resistivity. As more conductive ions diffuse into the formation with invasion, resistivity of the resident water changes in the direction favored by the concentration gradient between mud and formation.

5.2.2 Oil-saturated interval ($S_{wi} = S_{wr}$)

In oil-saturated intervals, formation water is at residual water saturation. In this case, transport of conductive ions is less likely to be the main mechanism that controls formation resistivity; instead, changing water saturation with time due to invasion becomes a more important phenomenon that controls resistivity. To get the saturation profiles with time during LOT, the invasion model discussed in Chapter 3 is used. Below is a plot of saturation profiles during LOT. Residual water saturation and residual oil saturation are both assumed to be 0.2.

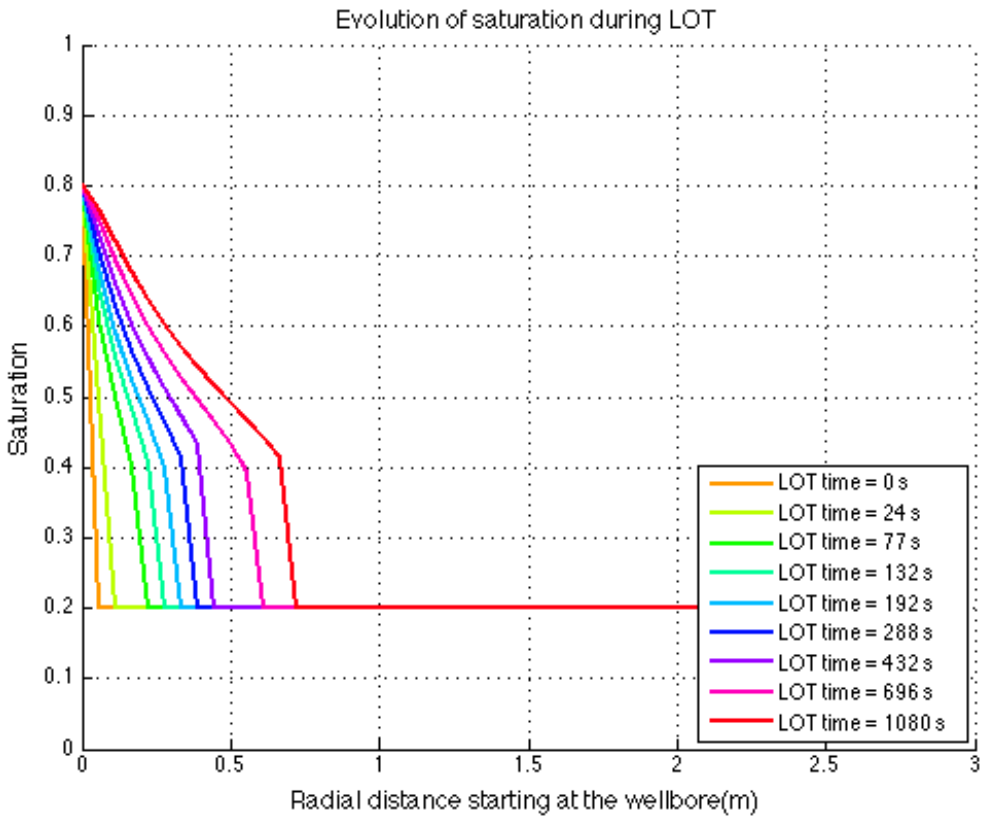

Fig 5.8 Formation water saturation during LOT (S_{wi} = 0.2)

As it can be seen in the figure, there is a saturation shock that propagates into the formation with time. This shock causes an abrupt change in water saturation at a certain radial distance from wellbore. This abrupt change in saturation must be manifested as a sharp change in resistivity of the formation at that location. This can be observed in the results reported in next section.

5.2.3 Arbitrarily-saturated interval ($S_{wi} \neq S_{wr}$, $S_{wr} < S_{wi} < (1- S_{or})$)

This case is similar to the oil-saturated case, but the effect of salinity change in initial formation water is not negligible. By superposing the effects of saturation change and salinity change, change in formation resistivity is determined. This is done for several values of arbitrarily picked initial water saturation values. Since the initial water saturation has changed, the shock saturation also changes, and sometimes, there might as well be no shock. Saturation profiles and concentration profiles for one example case of $S_{si} = 0.4$ is shown below.

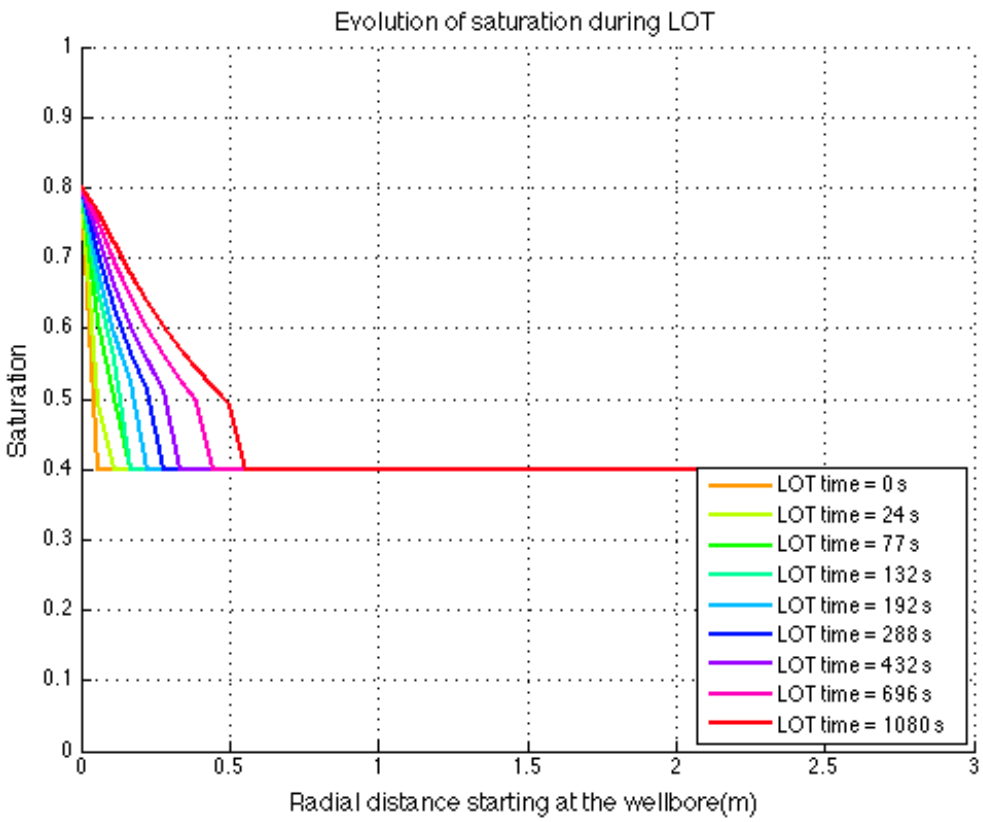

Fig 5.9 Formation water saturation during LOT (S_{wi} = 0.4)

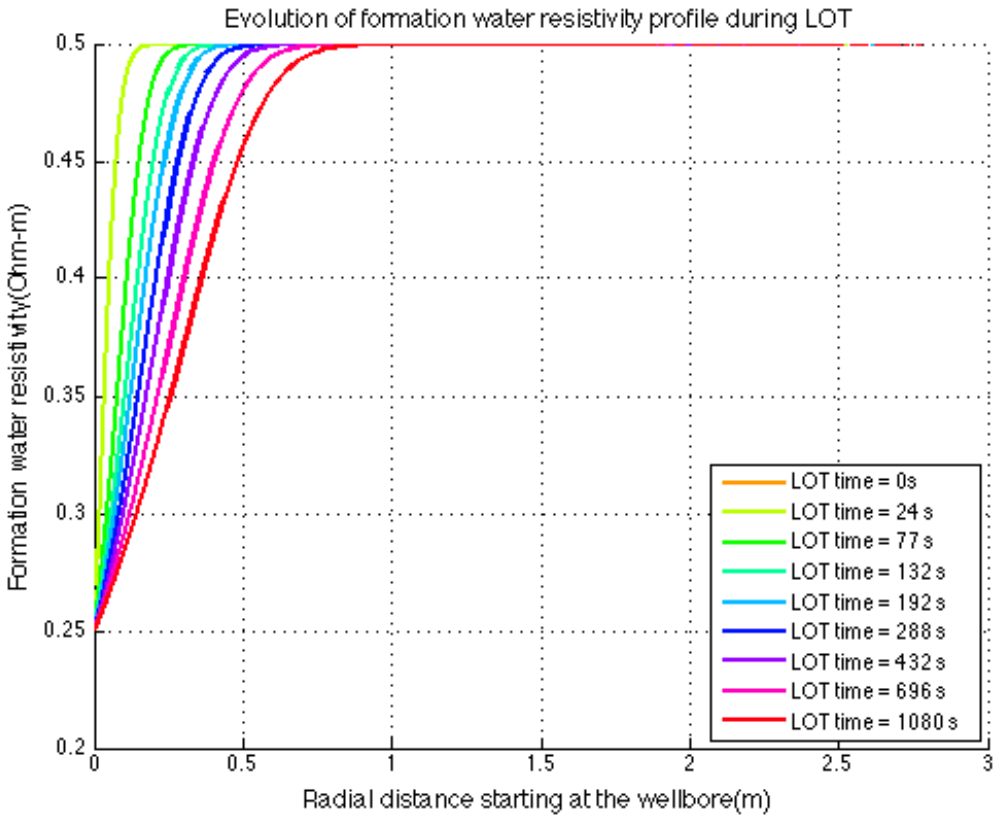

Fig 5.10 Resistivity of initially present formation water during LOT

Fig 5.9 shows the same profiles that are used for water-saturated case. The extent to which these profiles affect the equivalent formation water resistivity depends upon the extent to which water is initially present in the formation.

5.3 Combined effects of deformation and invasion on resistivity

The model is now ready to investigate the resistivity change around wellbore during LOT. Depending on the initial formation water saturation, either saturation change or salinity change can be the main mechanism to affect resistivity. In this section, resistivity change is investigated for different initial water saturation like it was done in the previous section.

5.3.1 Water-saturated interval ($S_{wi} = 1$)

The model now has everything that is needed to investigate resistivity in water-saturated interval. Since water saturation stays constant at 1, the simpler Archie's equation can be used to incorporate porosity change and salinity change into the model. Below is the plot of true formation resistivity change around wellbore for Trinidad U-3 assuming the tested interval to be water-saturated.

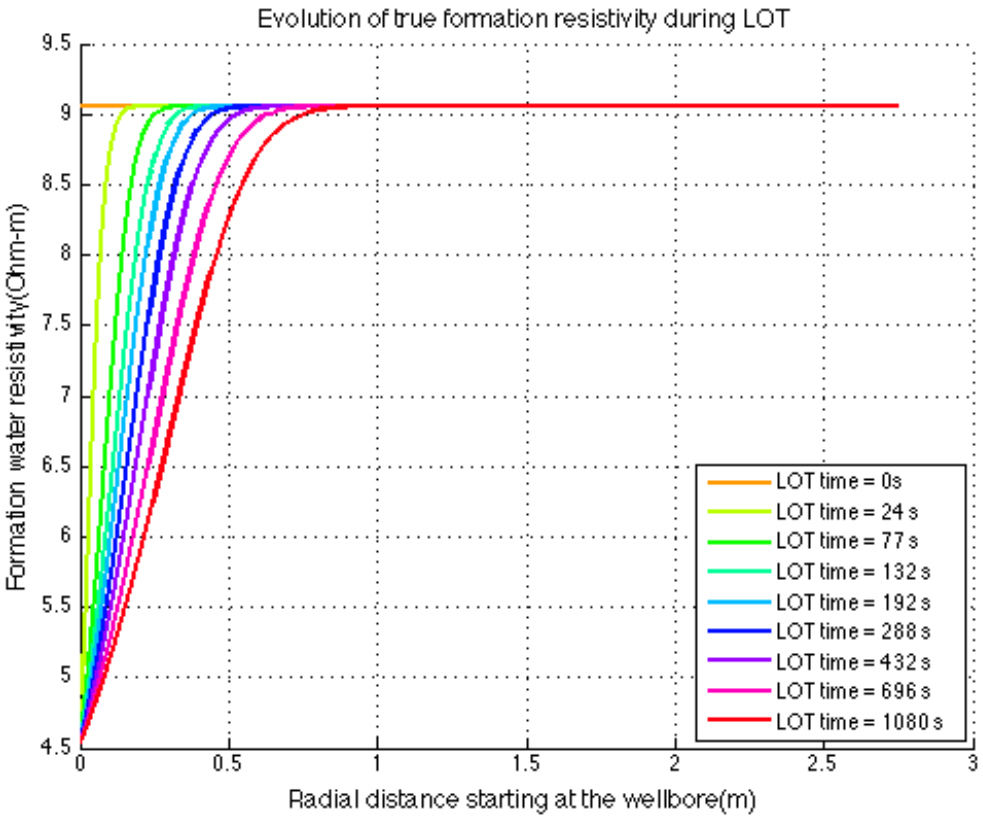

Fig 5.11 True formation resistivity around wellbore for Trinidad U-3 during LOT (assuming S_{wi}=1)

In case of water saturated interval, we see that the true formation resistivity changes smoothly radially outward. There is a considerable rise in resistivity within a certain location from wellbore depending upon the injection velocity and existing concentration gradient. After this point, the formation water resistivity is not affected by diffusion and advection; hence, the true formation resistivity also stays almost constant with deformation already negligible in this region.

5.3.2 Oil-saturated interval ($S_{wi} = S_{wr}$)

In oil-saturated interval, saturation change is the main mechanism behind resistivity change, and salinity change is supposedly less important. Nevertheless, two cases are investigated for comparison, at first ignoring the effect of diffusion in residual water, and then incorporating it. To do so, the concentration profiles obtained in the previous section are used to include the effects of diffusion. Obviously, when dispersion is ignored, shock front developed in saturation profile is manifested as an abrupt change in resistivity in that region. Fig 5.8 shows this phenomenon.

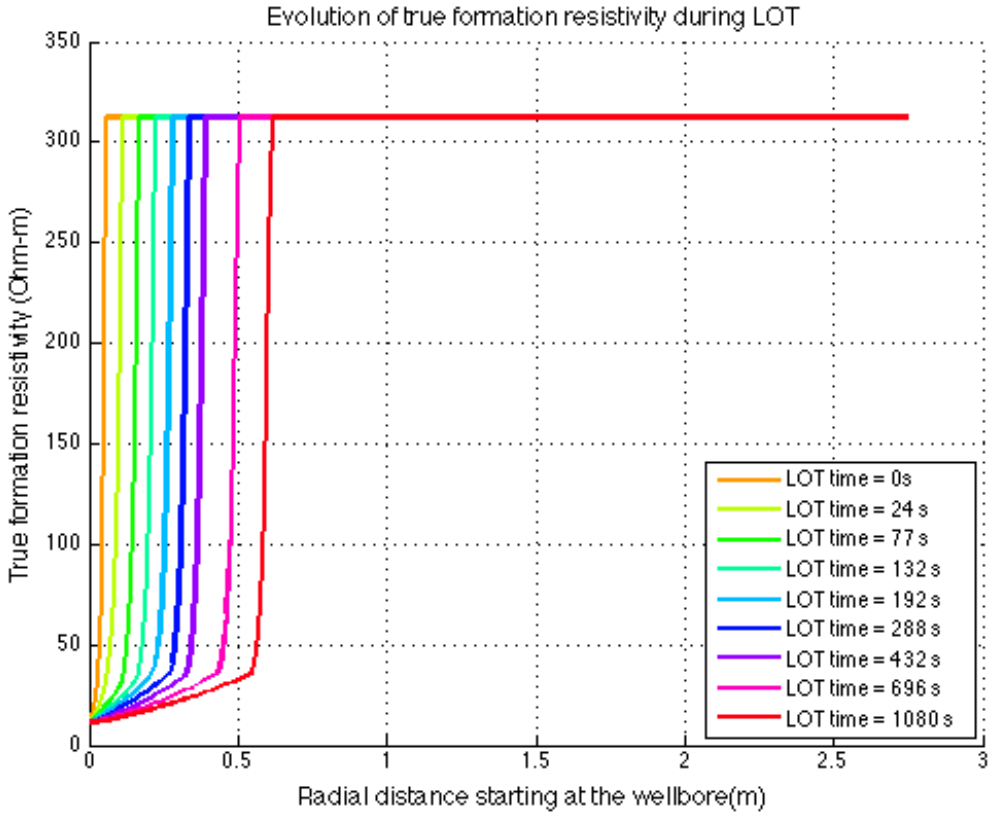

Fig 5.12 True formation resistivity around wellbore for Trinidad U-3 during LOT (assuming $S_{wi}=S_{wr} = 0.2$) (ignoring solute transport in residual water)

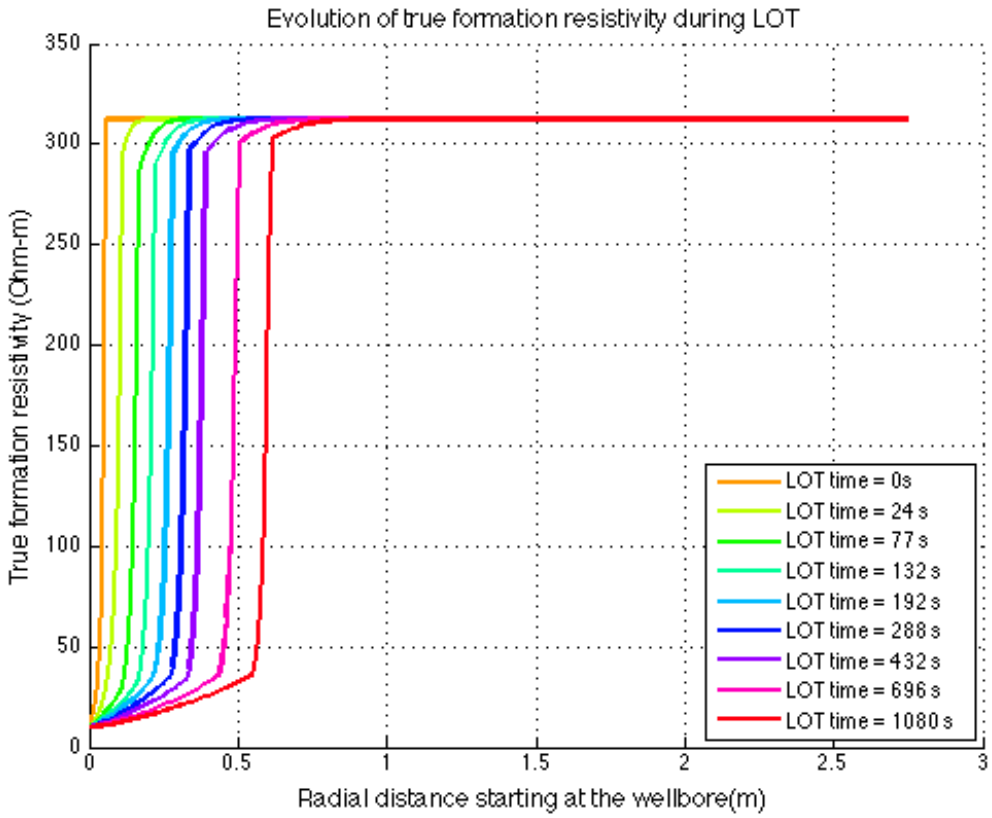

Fig 5.13 True formation resistivity around wellbore for Trinidad U-3 during LOT (assuming $S_{wi}=S_{wr} = 0.2$) (considering solute transport in residual water)

By comparing Figures 5.7 and 5.8 above, it is seen that considering diffusion and dispersion in residual water doesn't affect the final resistivity response by much. Only very close to the shock front, the effects of dispersion can be seen, as it smoothens out the abrupt change in resistivity due to saturation shock. Whether or not this is true for initial water saturation much higher than residual water saturation will be discussed in the next section.

Overall, when resistivity changes around wellbore during LOT on a water-saturated interval and an oil-saturated interval are compared, first thing that can be

noticed is the magnitude of change that happens in the two cases. In a water-saturated interval, even though equivalent formation water resistivity changes due to concentration gradient, saturation remains constant. Water saturation is a key parameter in Archie's equation. True formation resistivity can change greatly due to water saturation. Since this doesn't happen in a water- saturated interval, formation resistivity varies within a smaller range. On the contrary, in an oil-saturated interval, water saturation changes with time and causes the formation resistivity to change greatly. At the same time, equivalent formation water resistivity changes, as the fraction of invading fluid (with different resistivity) contributing towards total water saturation goes up with time. It must not be forgotten however that everything else remaining the same, initial formation resistivity for an oil-saturated interval is greater than that of water-saturated interval by more an order of magnitude. It is hence expected that the variation in that case is bigger in magnitude, since the range is wider.

5.3.3 Arbitrarily-saturated interval ($S_{wi} \neq S_{wr}$, $S_{wr} < S_{wi} < (1- S_{or})$)

Several initial water saturation values are arbitrarily picked to investigate the resistivity change around wellbore for each case. It is studied how incorporating or ignoring the contribution from solute transport affects the final results to determine what process dominates the change in resistivity during LOT when both mechanisms are relevant.

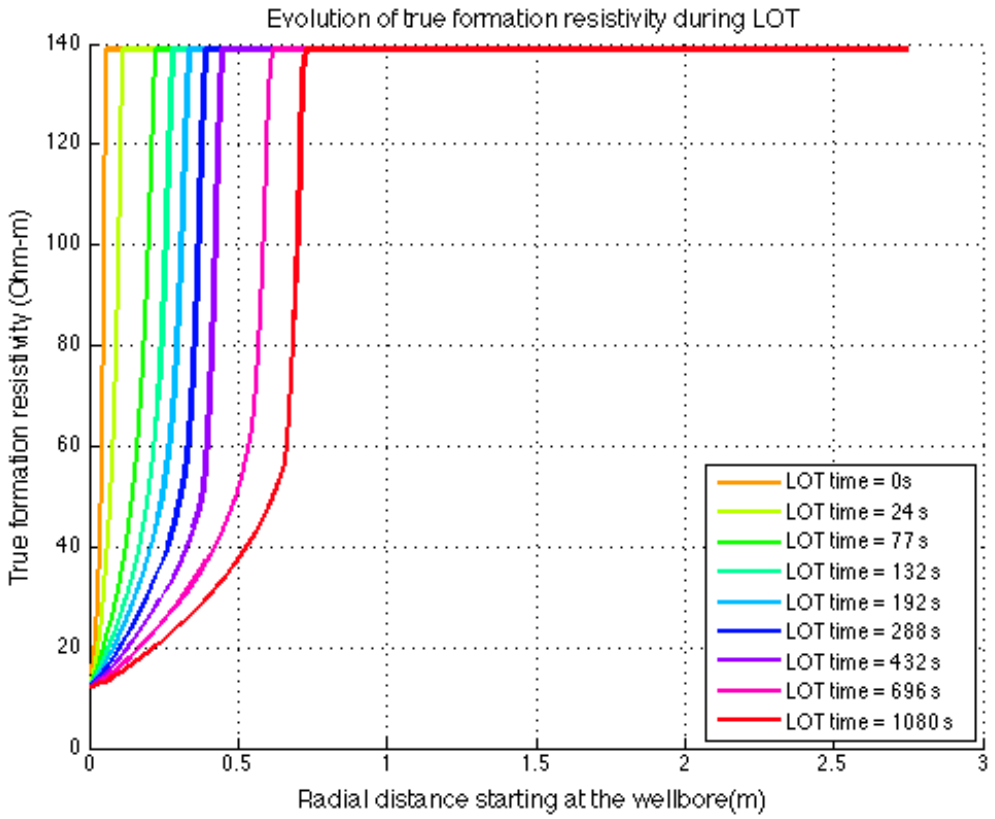

Fig 5.14 True formation resistivity around wellbore for Trinidad U-3 during LOT (assuming $S_{wi}=S_{wr} = 0.3$) (ignoring solute transport in initial water)

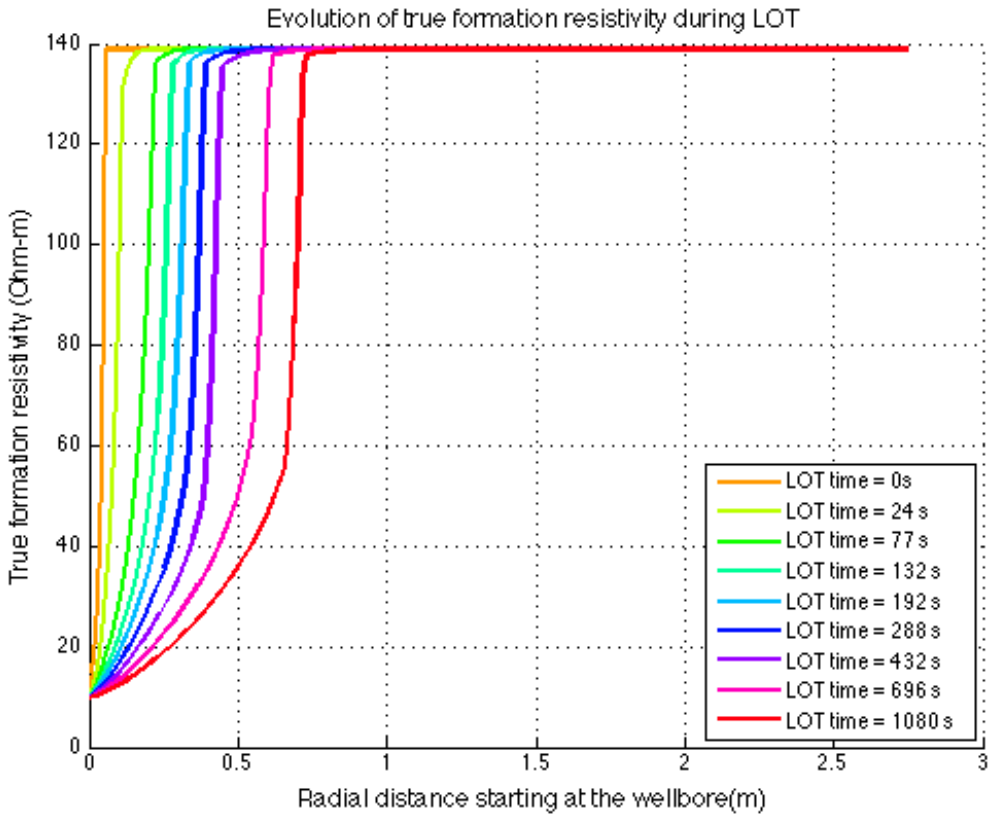

Fig 5.15 True formation resistivity around wellbore for Trinidad U-3 during LOT (assuming $S_{wi}=S_{wr} = 0.3$) (considering solute transport in initial water)

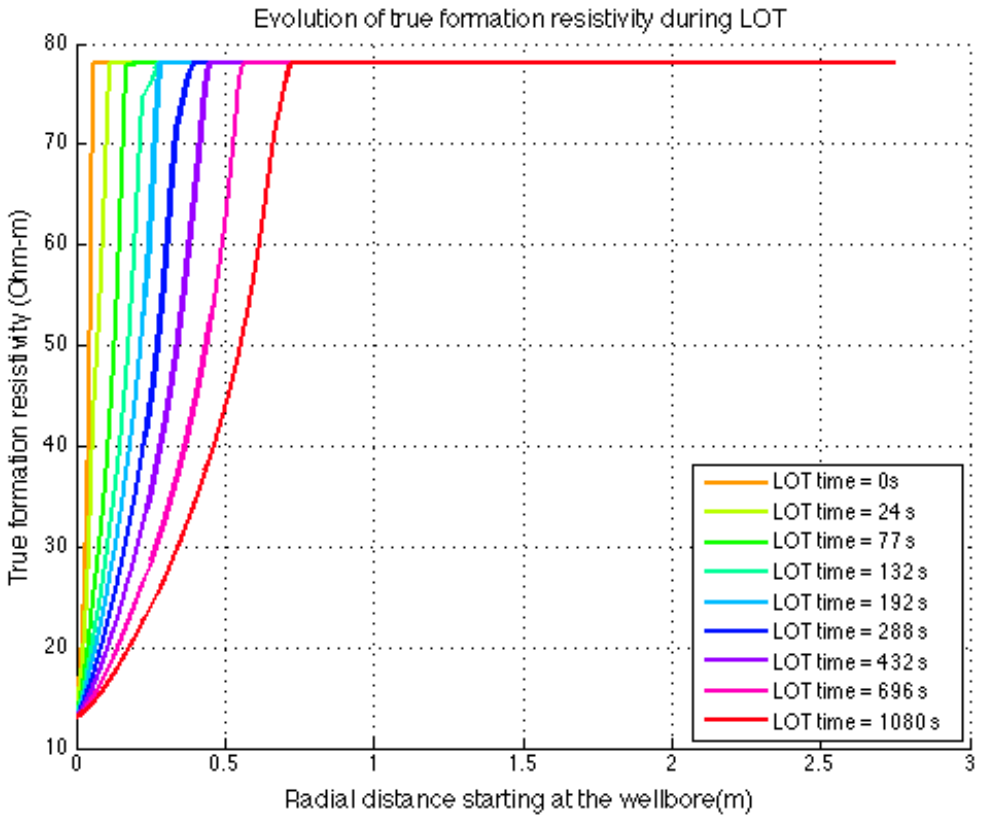

Fig 5.16 True formation resistivity around wellbore for Trinidad U-3 during LOT (assuming $S_{wi}=S_{wr} = 0.4$) (ignoring solute transport in initial water)

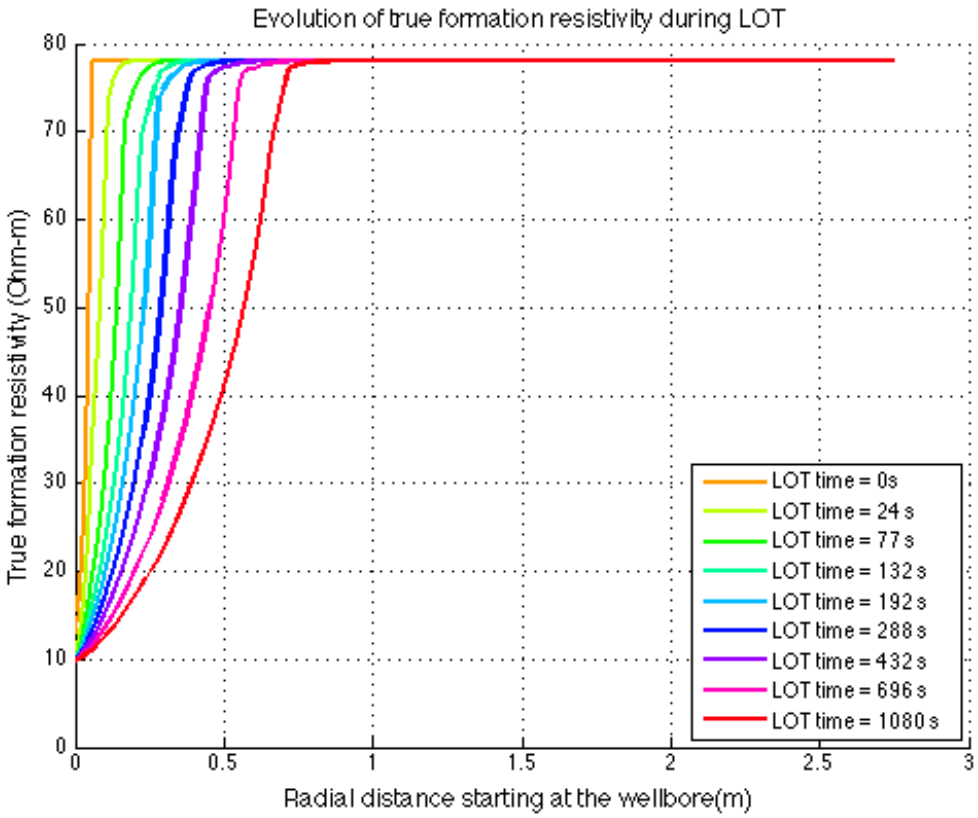

Fig 5.17 True formation resistivity around wellbore for Trinidad U-3 during LOT (assuming $S_{wi}=S_{wr} = 0.4$) (considering solute transport in initial water)

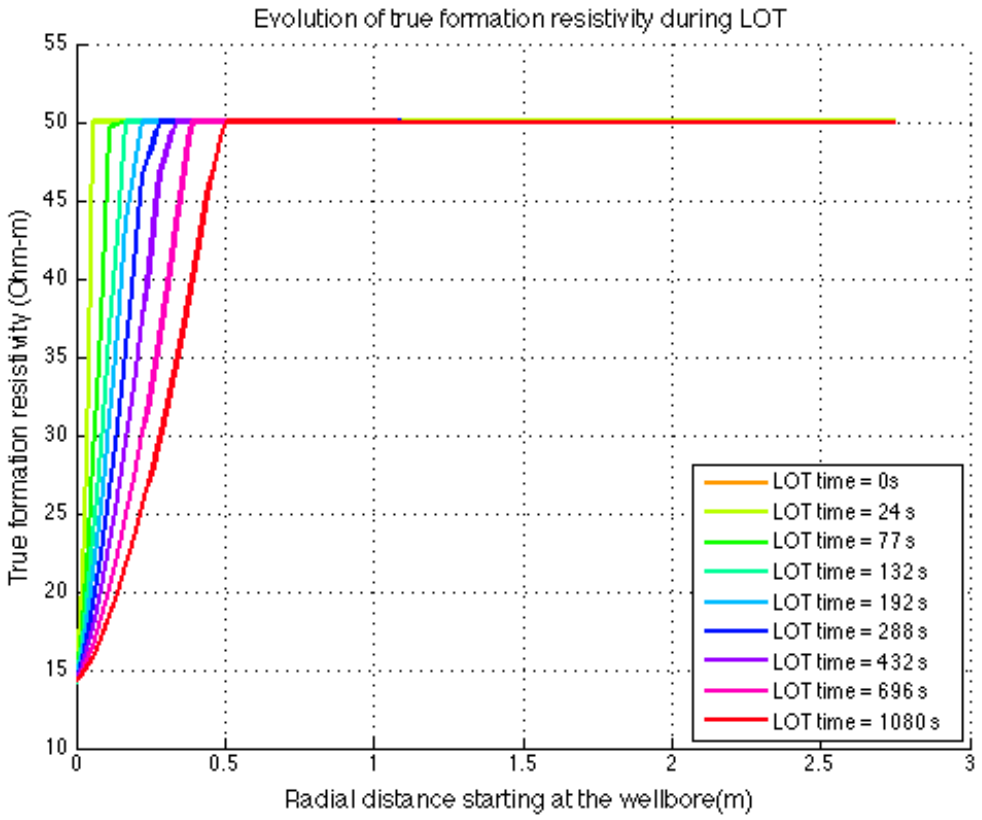

Fig 5.18 True formation resistivity around wellbore for Trinidad U-3 during LOT (assuming $S_{wi}=S_{wr} = 0.5$) (ignoring solute transport in initial water)

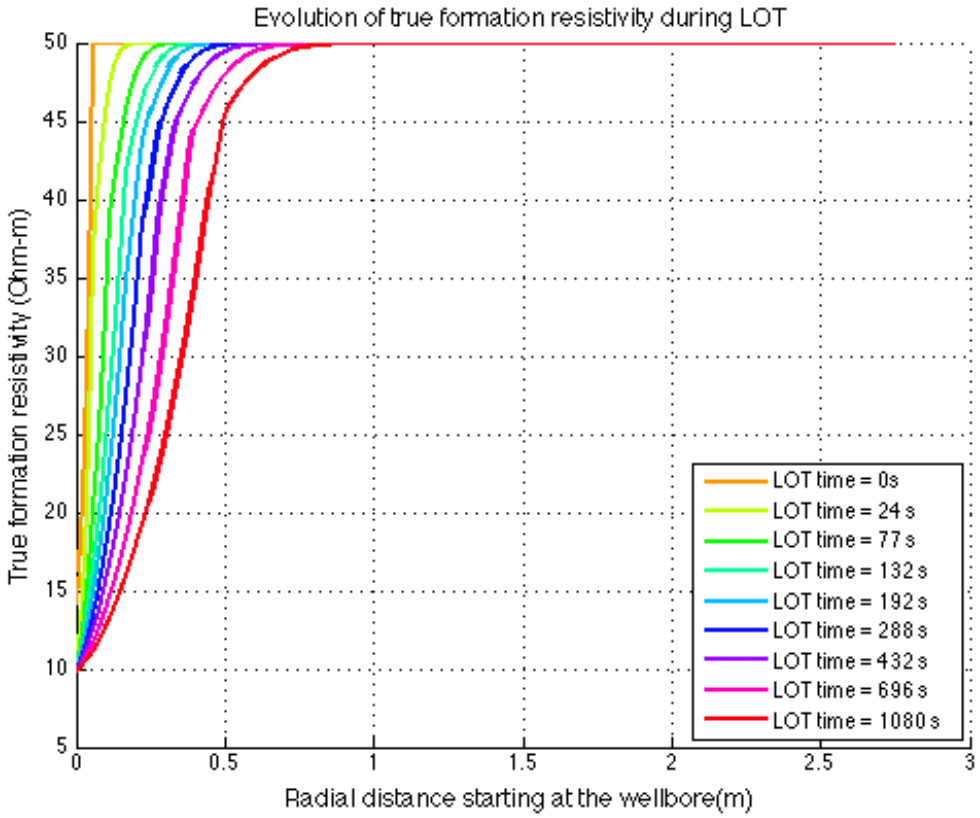

Fig 5.19 True formation resistivity around wellbore for Trinidad U-3 during LOT (assuming S_{wi}=S_{wr} = 0.5) (considering solute transport in initial water)

In the figures above, radial formation resistivity profiles are plotted for various initial formation water saturation values (i.e., S_{wi} = 0.3, 0.4, and 0.5). In each case, the effect of diffusion in initial formation water is first ignored and then included to see what difference it makes. From the plots, it can be seen that there is not a huge difference in the results with or without including the effects of salinity change even when the initial

water saturation is significantly greater than residual water saturation. This is a very important result, since it implies that when the saturation of the formation is changing, it predominantly dictates how the resistivity of the formation is going to change regardless of the effects of concentration gradient on water salinity. This is true, because formation resistivity has a greater dependence on saturation than salinity. Slight change in saturation can cause huge changes in formation resistivity, and any change in salinity can be overshadowed by the effect of saturation change on resistivity. One possible reason for this may be that any increase in saturation can significantly increase the overall connectivity of water in the pores and hence significantly alter the conductance. Changing the salinity of water in the pores does change the overall resistivity of rock by some amount, but since it does nothing to the connectivity of water in those pores, the effect might not be as big.

Chapter 6: Conclusion and Future Work

It has been successfully shown that resistivity change around wellbore can be investigated during LOT using our method of coupling the effects of deformation and invasion. Porous flow around wellbore is taken to be the effective phenomenon to model the leak-off behavior on average and thus investigate resistivity changes around wellbore during LOT. Depending on the initial reservoir condition (water saturation), different mechanisms can be responsible for affecting formation resistivity during LOT. While saturation change is a primary variable dictating resistivity change of the formation, in case if saturation is constant, concentration gradient in water becomes the main variable in case of a water-saturated zone. When both mechanisms are competing in an interval with arbitrary initial water saturation, saturation change seems to dominate and overshadow the effects of salinity change on overall formation resistivity.

Our approach enables us to model formation resistivity at any point in the formation at any time during LOT. Resistivity changes around the wellbore can thus be investigated as LOT progresses. In the next step, using the results from our model as input, resistivity tool response of a particular formation for a specific tool setting can be predicted during LOT. This involves solving another FEM problem based on Maxwell's equation to get the potential distribution in the tool electrodes, as resistivity around the wellbore changes during LOT.

One deficiency of our model is that it doesn't include fractures and assumes porous flow around the wellbore to be the effective phenomenon that can model leakage behavior during LOT on average. In future models, we plan to combine the porous flow mechanism with flow through pre-existing or LOT-induced fractures in order to have a more comprehensive model for resistivity change during LOT. In addition to that, we

plan to incorporate solid invasion and mud cake build up as well (Ramakrishnan & Wilkinson., 1997; Chenevert & Dewan, 2001).

References

Aadnoy, B. S., Mostafavi, V., & Hareland, G. (2009). Fracture Mechanics Interpretation of Leak-Off Tests. *Kuwait International Petroleum Conference and Exhibition*. Society of Petroleum Engineers.

Addis, M. A., Hanssen, T. H., Yassir, N., Willoughby, D. R., & Enever, J. (1998). A Comparison Of Leak-Off Test And Extended Leak-Off Test Data For Stress Estimation. *SPE/ISRM Rock Mechanics in Petroleum Engineering*. Trondheim, Norway: Society of Petroleum Engineers.

Altun, G. (1999). *Analysis of Non-linear Formation Fracture Resistance Tests Obtained During Oil Well Drilling Operations*. Baton Rouge: Lousiana State University.

Altun, G., Langlinais, J., & Bourgoyne Jr., A. (2001). Application of a new model to analyze leak-off tests. *SPE Drilling and Completion , 16* (02), 108-116.

Archie, G. E. (1942). The Electrical Resistivity Log as an Aid in Determining Some Reservoir Characteristics. *Transactions of the AIME , 146* (01), 54-62.

Arya, A., Hewett, T. A., Larson, R. G., & Lake, L. W. (1988). Dispersion and Reservoir Heterogeneity. *SPE Reservoir Engineering , 3* (01), 139-148.

Bailin, W. (2001). Boit's Effective Stress Coefficient Evaluation: Static And Dynamic Approaches. *ISRM International Symposium-2nd Asian Rock Mechanics Symposium* .

Biot, M. A., & Willis., D. G. (1957). The Theory of Consolidation. *J. Appl Elastic Coefficients of the Mech , 24* (1957), 594-601.

Chen, C. S. (1987). Analytical solutions for radial dispersion with Cauchy boundary at injection well. *Water Resources Research , 23* (7), 1217-1224.

Chen, C.-S., & Woodside, G. D. (1988). Analytical solution for aquifer decontamination by pumping . *Water Resources Research , 24* (8), 1329-1338.

Chenevert, M. E., & Dewan, J. T. (2001). A model for filtration of water-base mud during drilling: determination of mudcake parameters. *Petrophysics , 42* (03).

Cheng, A. D. (1997). Material coefficients of anisotropic poroelasticity. *International journal of rock mechanics and mining sciences , 34* (2), 199-205.

Cozzolino, K., & da Silva, J. D. (2007). Synthetic focusing and simulation of dual laterolog tool in axisymmetric subsurface models. *Journal of Applied Geophysics , 61* (2), 102-110.

Cozzolino, K., Howard, A. Q., & Protazio, J. S. (2000). A new look at multiphase invasion with applications to borehole resistivity interpretation. *Journal of applied geophysics , 43* (1), 91-100.

Crain, E. (n.d.). *Fracture identification*. Retrieved 10 28, 2015, from Crain's pterophysical handbook: https://www.spec2000.net/22-fracloc3.htm

Fallico, C., Chidichimo, F., & Straface, S. (2012). Solute dispersion in porous media at different transport velocities and distances. *International Water Technology Journal , 2* (2), 100-109.

Fu, Y. (2014). *Leak-Off Test (LOT) models* . The University of Texas at Austin, CPGE. The University of Texas at Austin.

Gandomkar, A., Fu, Y., & Gray, K. E. (2015). Leak-Off Test Model Combining Wellbore and Near-Wellbore Mechanical Behavior. *SPE Annual Technical Conference and Exhibition*. Society of Petroleum Engineer.

Heger, A., & Spoerker, H. (2011). Understanding XLOTs. *SPE/IADC Drilling Conference and Exhibition*. Amsterdam, The Netherlands: Society of Petroleum Engineers.

Hiby, J. W. (1962). Longitudinal and transverse mixing during single-phase flow through granular beds. *Proceedings of the Symposium on Interaction between Fluids and Particles* (pp. 312-320). London: nstitution of Chemical Engineers.

Hsieh, P. A. (1986). A new formula for the analytical solution of the radial dispersion problem. *Water Resources Research , 22* (11), 1597-1605.

Koval, E. J. (1963). A method for predicting the performance of unstable miscible displacement in heterogeneous media. *Society of Petroleum Engineers Journal , 3* (02), 145-154.

Lee, D., Bratton, T., & Birchwood, R. (2004). Leak-Off Test Interpretation and Modeling with Application to Geomechanics. *Gulf Rocks 2004, the 6th North America Rock Mechanics Symposium (NARMS)*. Houston, Texas: American Rock Mechanics Association.

Lee, M. W. (2002). Biot-Gassmann theory for velocities of gas hydrate-bearing sediments. *Geophysics , 67* (6), 1711-1719.

Li, G., Lorwongngam, A., & Roegiers, J. C. (2009). Critical Review Of Leak-Off Test As A Practice For Determination Of In-Situ Stresses. *43rd US Rock Mechanics Symposium & 4th US-Canada Rock Mechanics Symposium*. American Rock Mechanics Association.

Luo, X., Were, P., Liu, J., & Hou, Z. (2015). Estimation of Biot's effective stress coefficient from well logs. *Environmental Earth Sciences , 73* (11), 7019-7028.

Miller, S. F., & King, C. J. (1966). Axial dispersion in liquid flow through packed beds. *AIChE Journal , 12* (4), 767-773.

Nam, M. J., Pardo, D., & Torres-Verdín, C. (2008). Simulation of DC dual-laterolog measurements in complex formations: A Fourier-series approach with nonorthogonal coordinates and self-adapting finite elements. *Geophysics , 74* (1), E31-E43.

Norris, T. (n.d.). *Algorith Derivation*. Retrieved 9 10, 2015, from Toby Norris's Website: http://www.tobynorris.com/work/prog/cpp/mfc/concyl_hlp/algorithmderivation.htm

Okland, D., Gabrielsen, G. K., Gjerde, J., Koen, S., & Williams, E. L. (2002). The importance of extended leak-off test data for combatting lost circulation. *SPE/ISRM Rock Mechanics Conference*. Society of Petroleum Engineers.

Paknejad, A., Schubert, J., & Amani, M. (2007). A New Method to Evaluate Leak-Off Tests in Shallow Marine Sediments (SMS). *SPE Saudi Arabia Section Technical Symposium*. Society of Petroleum Engineers.

Pardo, D., Calo, V. M., Torres-Verdin, C., & Nam, M. J. (2008). Fourier series expansion in a non-orthogonal system of coordinates for the simulation of 3D-DC borehole resistivity measurements. *Computer Methods in Applied Mechanics and Engineering , 197* (21), 1906-1925.

Peters, E. J. (2012). *Advanced Petrophysics* (Vol. 2). Greenleaf Book Group.

Postler, D. P. (1997). Pressure Integrity Test Interpretation. *SPE/IADC Drilling Conference*. Amsterdam: Society of Petroleum Engineers.

Poulsen, T. G., Suwarnarat, W., Hostrup, M. K., & Kalluri, P. N. (2008). Simple and rapid method for measuring gas dispersion in porous media: Methodology and applications. *Soil science , 173* (3), 169-174.

Ramakrishnan, T. S., & Wilkinson., D. J. (1997). Formation producibility and fractional flow curves from radial resistivity variation caused by drilling fluid invasion. *Physics of Fluids (1994 to present) , 9* (4), 833-844.

Rosthal, R. A., Young, R. A., Lovell, J. R., Buffington, L., & Arceneaux, C. L. (1995). Formation Evaluation and Geological Interpretation from the Resistivity-at-the-Bit Tool. *SPE Annual Technical Conference and Exhibition*. Society of Petroleum Engineers.

Tang, D. H., & Babu, D. K. (1979). Analytical solution of a velocity dependent dispersion problem. *Water Resources Research , 15* (6), 1471-1478.

Torres-Verdin, C. (2013, 1). Well-log Compendium for Instruction of Fundamentals of Well Logging.

van Oort, E., & Vargo, R. F. (2007). Improving Formation Strength Tests and Their Interpretation. *SPE/IADC Drilling Conference*. Amsterdam, The Netherlands: Society of Petroleum Engineers.

Veling, E. (2001). Analytical solution and numerical evaluation of the radial symmetric convection-diffusion equation with arbitrary initial and boundary data. *IAHS PUBLICATION* , 271-276.

Wang, H., Sweatman, R. E., Engelman, R., Deeg, W. F., Whitfill, D. L., Soliman, M. Y., et al. (2008). Best practice in understanding and managing lost circulation challenges. *SPE Drilling & Completion , 23* (02), 168-175.